

To Print: Click your browser's PRINT button.

NOTE: To view the article with Web enhancements, go to:

<http://www.medscape.com/viewarticle/513716>

MRI of Articular Cartilage: Revisiting Current Status and Future Directions

Michael P. Recht; Douglas W. Goodwin; Carl S. Winalski; Lawrence M. White

Am J Roentgenol. 2005;184(4):899-914. ©2005 American Roentgen Ray Society

Posted 10/03/2005

Abstract and Introduction

Abstract

Objective: The Purpose of this article is to review the current understanding of the MRI appearance of articular cartilage and its relationship to the microscopic and macroscopic structure of articular cartilage, the optimal pulse sequences to be used in imaging, the appearance of both degenerative and traumatic chondral lesions, the appearance of the most common cartilage repair procedures, and future directions and developments in cartilage imaging.

Conclusion: Articular cartilage plays an essential role in the function of the diarthrodial joints of the body but is frequently the target of degeneration or traumatic injury. The recent development of several surgical procedures that hold the promise of forming repair tissue that is hyaline or hyalinelike cartilage has increased the need for accurate, noninvasive assessment of both native articular cartilage and postoperative repair tissue. MRI is the optimal noninvasive method for assessment of articular cartilage.

Introduction

MRI of articular cartilage has attracted intense interest and been the subject of numerous research studies over the past several years. There are several reasons: the essential role articular cartilage plays in the function of the diarthrodial joints of the body, the high prevalence of degeneration and traumatic injury of articular cartilage, and the recent development of new surgical procedures that hold the promise of forming repair tissue that is hyaline or hyalinelike cartilage. In 1994, a review article in *AJR*, "MR Imaging of Articular Cartilage: Current Status and Future Directions," summarized early experience with MRI of articular cartilage by stating that "although the role of MRI in the evaluation of articular cartilage remains undefined, this imaging method has great promise and may emerge as an effective technique for detecting even the early stages of chondral abnormalities".^[1] Over the past 10 years, studies have shown that although initial understanding of the MRI appearance of articular cartilage may have been limited and the pulse sequences used to evaluate articular cartilage suboptimal, MRI is indeed the optimal diagnostic method for evaluation of articular cartilage. MDCT, with its superior resolution, may play a role in the future imaging of articular cartilage, but that role has yet to be defined. MRI plays a significant role not only in diagnosis of chondral lesions but also in determination of the appropriate surgical or pharmacologic treatment and evaluation of such treatment. This article discusses the current understanding of the MRI appearance of articular cartilage and its relationship to the microscopic and macroscopic structure of articular cartilage, the optimal pulse sequences to be used, the appearance of both degenerative and traumatic chondral lesions, the appearance of the most common cartilage repair procedures, and future directions and developments of cartilage imaging.

MRI Appearance of Normal Articular Cartilage

Layers or laminae of varying signal intensity are the characteristic feature of MR images of normal articular cartilage (Figs. 1A and 1B). When images are acquired with the articular surface perpendicular to the main magnetic field (B_0), a higher-signal-intensity transitional layer separates the low-signal-intensity surface from a low-signal-intensity deep layer adjacent to the subchondral bone. These layers reflect the continuous variation in T2 values across the thickness of the tissue.^[2] T1, diffusion, and proton density have only minimal influence on tissue contrast.^[3-7] The minimum T2 relaxation time in articular cartilage is short—approximately 10 msec. As a result, T2 is the determinant of tissue contrast even on T1-weighted and proton density-weighted images.^[2,5,8] On short-TE images acquired with gradient-echo sequences or projection reconstruction techniques, the influence of T2 relaxation can be minimized, producing cartilage images with uniform signal intensity.^[9-11] Truncation effects, however, may cause an appearance similar to the layers seen on longer-TE images.^[6,12] Magnetization transfer effects may also alter the laminar appearance on multiecho fast spin-echo images by decreasing signal intensity.^[13]

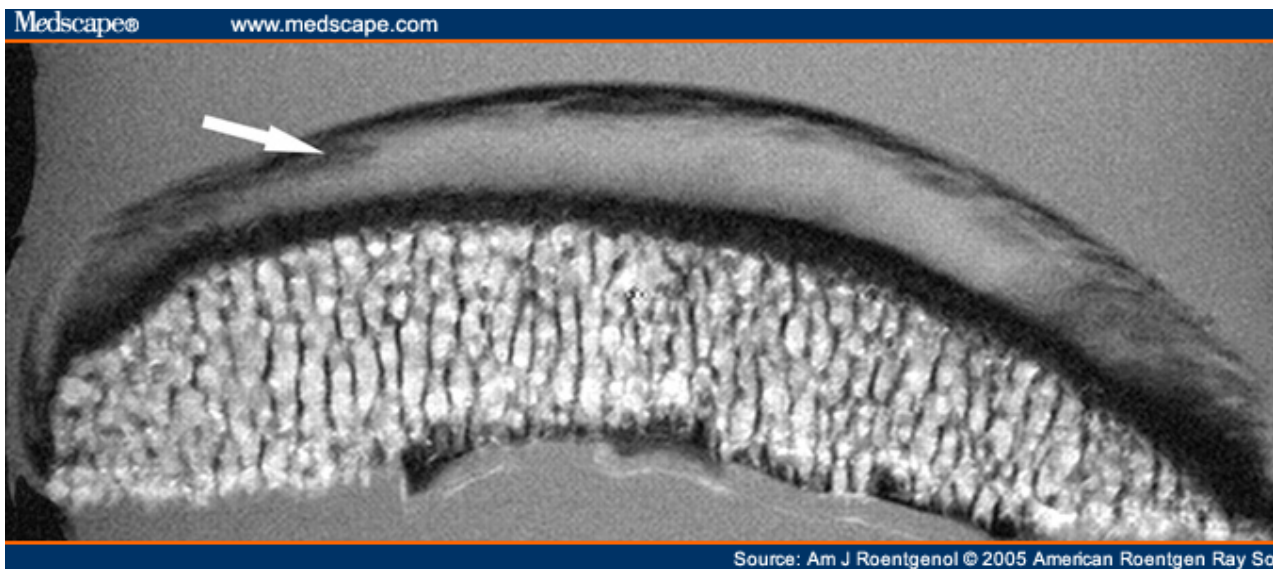
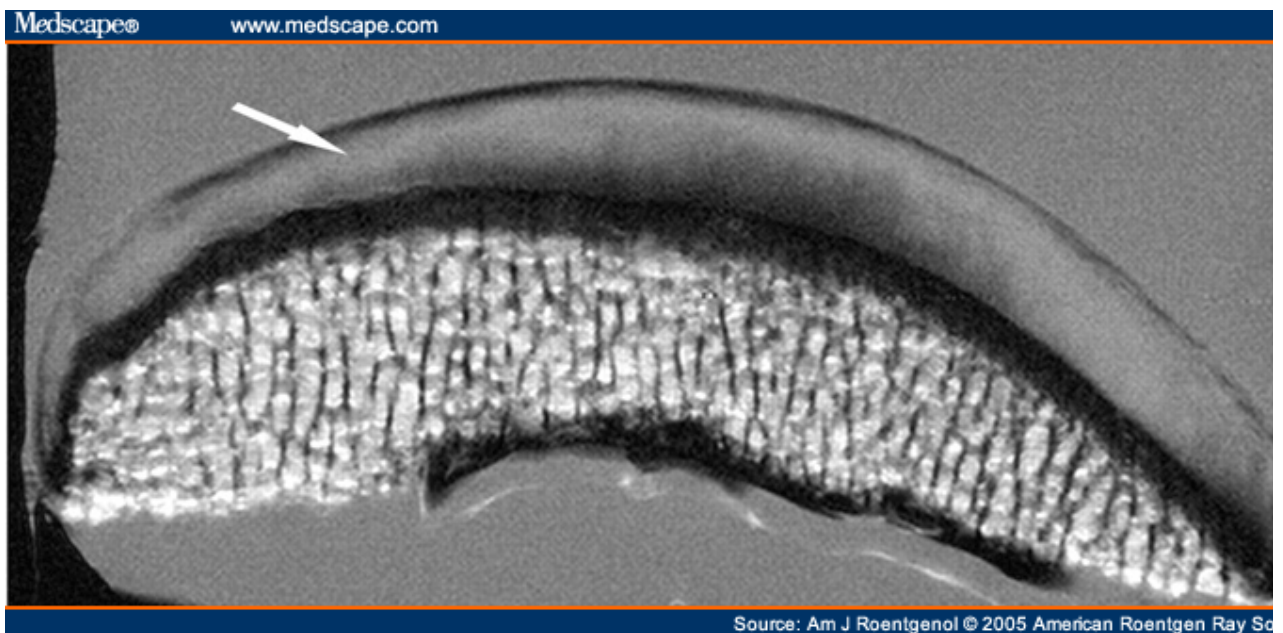


Figure 1.

In 65-year-old woman, spin-echo images (TR/TE, 1,000/20) of femoral condyle fragment imaged at 7 T with articular surface perpendicular to (A) and parallel with (B) main magnetic field. (Reprinted with permission from^[21])

A, Higher-signal-intensity transition layer (*arrow*) separates lower-signal-intensity radial layer from low-signal-intensity surface.

B, When imaged after rotation of sample by 90°, pattern of layering changes shows influence of magic-angle effect. Orientation effect is evident at all levels of sample, including transitional layer (*arrow*).

Although cartilage appears relatively uniform on gross inspection, the orientation of collagen and the concentration of water, chondrocytes, and proteoglycans varies across the thickness of the tissue.^[14,15] The presence of layers in cartilage seen on MR images suggests a correlation with histologic zonal organization. Rubenstein et al.^[16] established a link between tissue structure and the MR image by demonstrating T2 anisotropy within cartilage. In their study, the pattern of layering seen on MR images varied as cartilage orientation relative to B0 changed, proving that the influence of structural elements within cartilage was responsible for the presence of layering. Within highly structured tissues such as cartilage, the restriction of water mobility and the resulting enhancement of dipole interactions shorten T2 relaxation. In such tissues, however, T2 relaxation is dependent not only on the distance between nuclei but also on orientation relative to B0. As the internuclear vector is angled away from B0, T2 lengthens, reaching a maximum effect at approximately 54.7°.^[17-19] This influence of orientation is commonly referred to as the magic-angle effect.

Investigations into the influence of orientation on T2 and cartilage layers led to speculation that regional differences in the orientation of collagen fibrils could explain the T2 heterogeneity (layers) and anisotropy (orientation dependence).^[2,16] Microscopy studies have shown that collagen fibrils are oriented in parallel arrays perpendicular to the subchondral bone in the deepest level of cartilage and horizontal to the surface superficially. A transitional zone of randomly oriented fibrils separates these two regions or zones.^[15] Such an organization would explain the short T2 and anisotropy in the deep layer and surface on MR images of cartilage and the longer T2 and apparent lack of anisotropy in the transitional layer on MR images.

The assertion that regional variations in collagen fibril orientation could determine the T2 heterogeneity of cartilage is compelling, yet no direct correlation between the histologic and MRI findings has established such a link. Moreover, there appear to be several difficulties with this explanation. First, the layers seen on MR images are not well defined and instead represent gradual changes in the bell-shaped T2 profile of cartilage.^[2] Accordingly, the thickness of layers is determined by the TE: On images acquired with a longer TE, the width of the higher-signal-intensity transitional layer decreases.^[4] Second, as Grunder et al.^[20] reasoned, the predicted influence of collagen fibrils on water should be too weak to explain the strong effects observed on orientation. Finally, anisotropy has been shown in all layers of cartilage^[21] (Figs. 1A and 1B). The structural elements that determine T2 must therefore be present across the entire thickness of the tissue.

An alternative theory explaining the relationship between cartilage morphology and the MRI appearance of cartilage becomes apparent if one considers the structure of cartilage at the macroscopic rather than microscopic level. Collagen fibrils, proteoglycans, and the other constituents of the extracellular matrix of cartilage are organized into a larger continuous macroscopic structure that radiates from the subchondral bone and curves into the plane of the articular surface (Figs. 2A and 2B). Fracture sectioning, typically used to prepare cartilage for scanning electron microscopy, causes cartilage to separate along lines of least resistance, thereby reflecting the tissue organization in the plane of the fracture.^[22] The curved structure revealed by the fracture is variably referred to in the microscopy literature as fibers, layers, or leaves.^[21-25] Differences in the description of this macroscopic structure likely reflect interspecies variation, differences in fracture technique, and unavoidable artifacts.^[22]

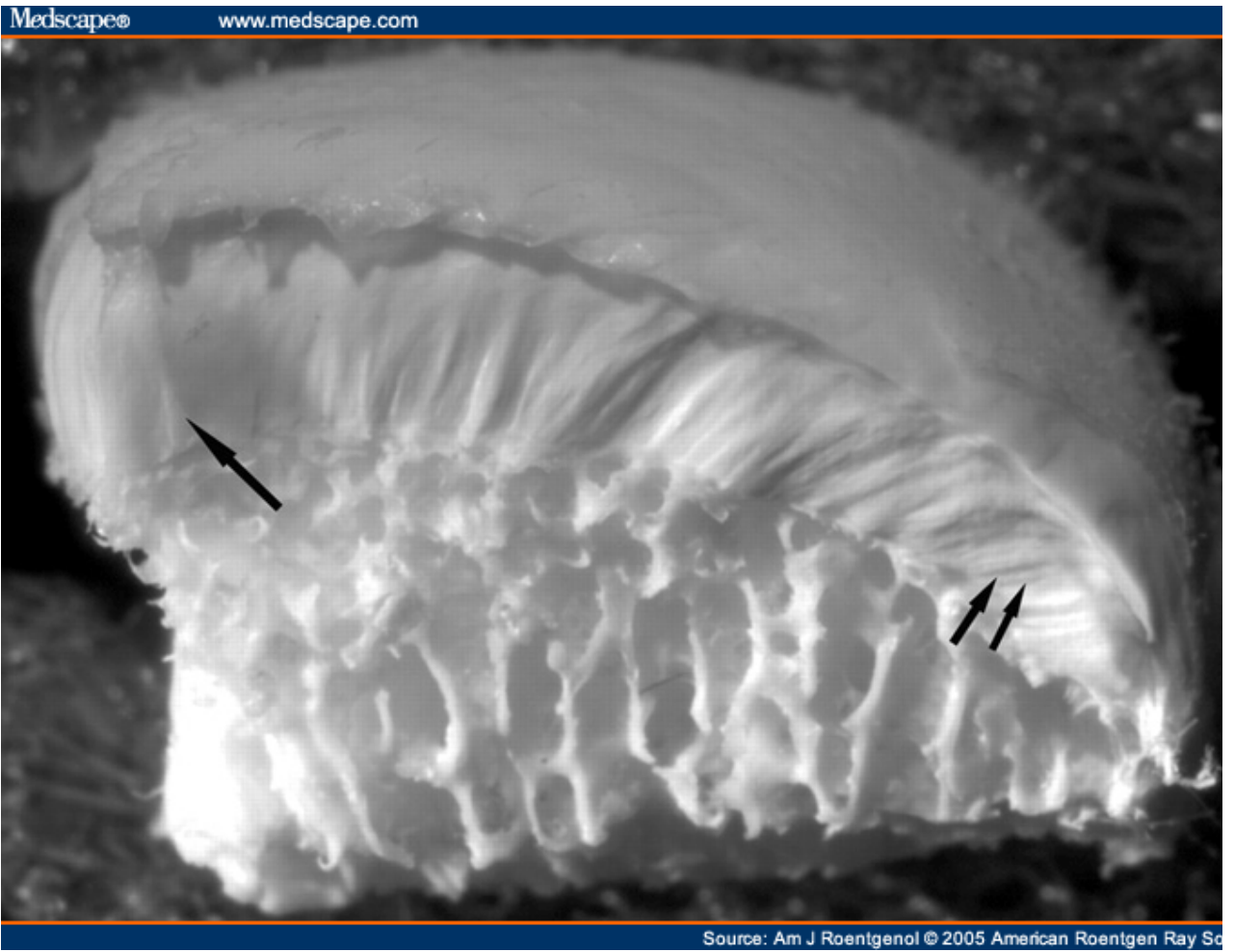
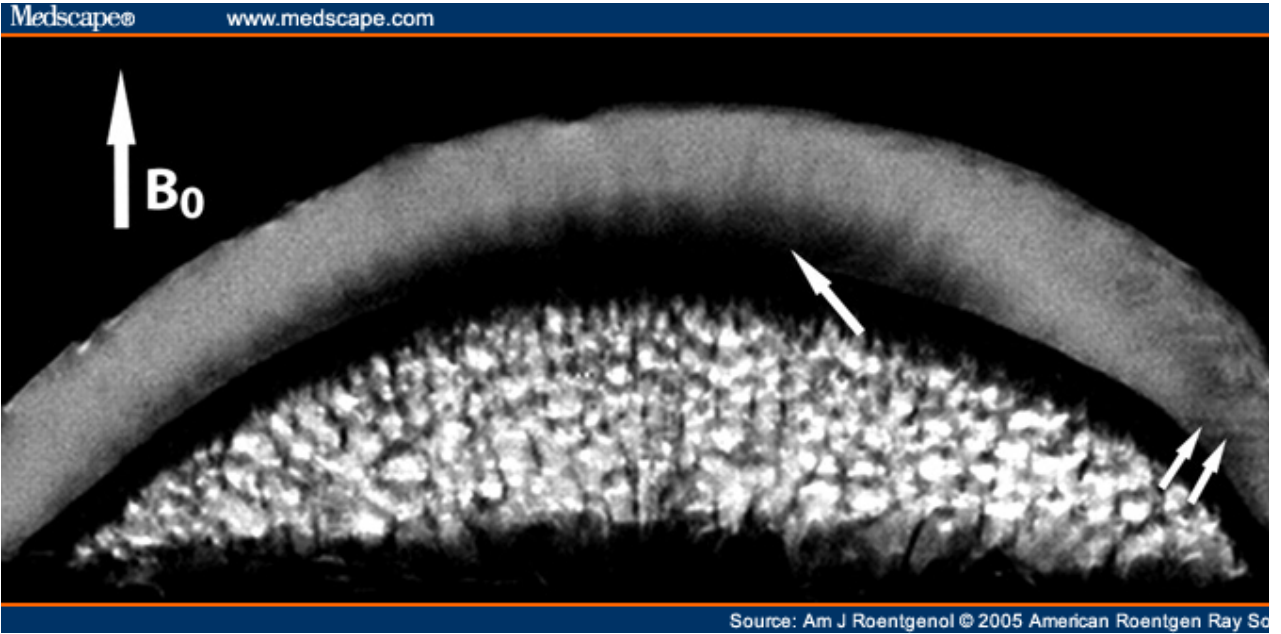


Figure 2.

Osteochondral fragment from 56-year-old man. (Reprinted with permission from^[32])

A, Spin-echo image (TR/TE, 1,000/20) of femoral condyle fragment imaged at 7 T shows low signal intensity (*arrows*) in regions where cartilage matrix is aligned with main magnetic field (B_0).

B, Sample photographed after fracture sectioning. In regions where cartilage matrix is aligned with B_0 , signal intensity is low (*long arrow*). Striations on MR image appear to reflect fibrous-appearing structure revealed in fractured sample (*short arrows*).

Given the presence of a continuous structure radiating from the subchondral bone and arcing into the plane of the joint surface, the magic-angle effect provides an excellent explanation for T2 heterogeneity and anisotropy in cartilage.^[21,26,27] As the macroscopic structure of cartilage curves away from B_0 , T2 gradually increases, reaching a peak in the middle of the transitional layer where tissue alignment is 55° . As the tissue continues to curve into the plane of the articular surface, T2 shortens. Fibrous columnlike structures seen on the surface of sectioned samples of fractures appear to correlate with striations within low-signal-intensity MRI layers^[26,27] (Figs. 2A and 2B), suggesting that MRI is also capable of revealing macroscopic structure at an even more detailed level.

The apparent lack of anisotropy reported in the transitional layer on a number of studies is predictable if one considers the complexity of cartilage structure and the limitations of MRI. When a sample of cartilage is tilted 55° , only portions of the curved cartilage will then be oriented parallel to B_0 . Given the relatively thick slices used for MRI, T2 measurements of a curved tissue oriented at an angle will include a mixed population of tissue orientations and resulting T2 values. The failure to show anisotropy should therefore not be considered proof that it does not exist.

Early investigations of cartilage histology suggested that the structure of cartilage is joint-specific.^[28] Split lines, created in articular surfaces by puncturing the cartilage with a round pin, are arranged in patterns that are characteristic for individual joints.^[28,29] Later investigations established that the shape of the underlying matrix determines split-line orientation.^[23] Split lines are, in effect, the most superficial aspect of a fracture plane. Surface split-line patterns therefore reflect the organization of the entire extracellular matrix of the cartilage of a particular joint. The predictability of split-line patterns suggests that variations in matrix structure are also predictable. Joint-specific and reproducible variations in the shape of the tibial plateau matrix, suggesting a characteristic structure or architecture, have been reported.^[24]

Because of the strong influence of matrix structure on T2 contrast, the appearance of articular cartilage on MR images should also be characteristic or joint-specific. This specificity has been shown at the tibial plateau in a study documenting characteristic and reproducible variations in T2 and signal intensity that correlate well with an equally characteristic matrix architecture.^[30]

Regional variations in the MRI appearance of cartilage should also be expected in other joints. Unfortunately, this variability in cartilage structure complicates efforts to develop standardized Methods of monitoring cartilage injury, degeneration, and repair. In a recent study, for example, a failure to account for variability in cartilage structure likely explains the observation of orientation effects on T2 measurements that were substantially less than expected.^[31,32] On the other hand, the strong influence of structure on MR image contrast indicates that MRI is ideally suited to the evaluation of tissue integrity. Although current clinical imaging sequences cannot reliably show early changes of cartilage anatomy and composition, new techniques (which are discussed later in this article) hold promise for being able to detect such changes.

Critical factors that affect the MRI evaluation of articular cartilage include image spatial resolution, image signal-to-noise ratio (SNR), and the choice of image acquisition protocol. The advent and clinical validation of pulse sequences optimized for the MRI assessment of

articular cartilage have provided the opportunity to confidently assess the status of articular cartilage along with other articular structures on routine clinical imaging.

A number of different clinically available pulse sequences can be used in MRI of cartilage, with each technique taking advantage of differing contrast characteristics of cartilage and adjacent tissue and affecting overall image spatial resolution and image SNR. The most widely used and accurate of these cartilage-specific sequences include spoiled gradient-recalled echo (SPGR) and fast spin-echo imaging.

Three-dimensional T1-weighted SPGR acquisitions provide high-resolution contiguous thin-slice images in shorter scan times than can conventional spin-echo techniques. Fat-suppressed SPGR images show high contrast between bright cartilage and relatively dark fluid, bone, fat, and muscle. The adjunct use of fat suppression with this and other cartilage-imaging pulse sequences has been advocated as a means of increasing the dynamic range of signal intensity throughout the image, potentially allowing for better detection of subtle signal-intensity alterations.^[33,34] With 3D SPGR imaging, cartilage abnormalities are seen as morphologic abnormalities of cartilage contour. Fat-saturated 3D SPGR imaging has been shown to be more accurate than standard spin-echo MRI in the detection of cartilage defects in the knee, with sensitivities of as high as 93%.^[35-39] Limitations of the technique include relatively long acquisition times compared with those of fast spin-echo imaging sequences. Possible techniques to decrease imaging times include half-Fourier techniques and fat suppression using spatial-spectral excitation pulses.^[40,41] An additional potential disadvantage of gradient-recalled echo imaging is its relative sensitivity to susceptibility artifacts and intra-voxel dephasing, which may compromise image quality in the setting of postoperative surgical debris or hardware in patients who underwent prior arthroscopic surgery or prior cartilage reparative procedures.

Fast spin-echo imaging techniques allow high-resolution images to be acquired in a relatively short time. Fast spin-echo imaging of cartilage benefits, in addition, from inherent magnetization transfer effects within normal cartilage, potentially increasing the relative conspicuity of cartilage abnormalities.^[14,42,43] Both intermediate- and T2-weighted fast spin-echo imaging sequences, with and without fat suppression, have been advocated in the assessment of articular cartilage integrity.^[44-48] With such imaging, cartilage appears intermediate in signal intensity and joint fluid appears bright in signal intensity. Cartilage abnormalities can be seen as areas of morphologic contour defects or as regions of relatively increased intrasubstance-cartilage signal intensity^[49,50] most likely reflective of increased intracartilaginous free water and collagenous ultrastructure disruption.^[51,52] Similar to the Results for investigations of SPGR imaging, fast spin-echo imaging has been shown to have sensitivities of as high as 94% in the detection of arthroscopically documented cartilage disease.^[46] Of clinical importance, fast spin-echo imaging techniques have been shown, in addition, to be valuable pulse sequences in the diagnostic evaluation of other intraarticular structures including menisci, ligaments, and subchondral bone.^[53-55] Disadvantages of typical 2D fast spin-echo imaging acquisitions include limited through-plane resolution relative to 3D SPGR imaging and the potential for image-blurring artifacts on short-TE-weighted acquisitions as a result of high-spatial-frequency-encoding echoes late in the fast spin-echo echo train. Practical problems related to fast spin-echo blurring, however, may be minimized through appropriate minimization of interecho spacing and the use of short echo-train lengths. MR arthrography has been advocated particularly for the evaluation of cartilage repair procedures because of the ability of contrast material to outline the surface of and enter defects within repair tissue. Few studies have been performed on the use of MR arthrography in cartilage repair procedures, but indirect MR arthrography has been found to better define the surface of repair tissue and differentiate between intact repair tissue and delaminated tissue in patients after autologous chondrocyte implantation (ACI).^[56,57]

Numerous variations of these imaging techniques exist, with imaging parameters and acquisition sequences varying between centers on the basis of multiple factors, including user preferences and the potential strengths and weaknesses of available vendor hardware platforms. In general, practical MRI protocols for evaluation of hyaline articular cartilage include at least one cartilage-sensitive sequence obtained in the sagittal plane. Sagittal

acquisitions allow imaging assessment of cartilage in an orientation generally perpendicular to the majority of weight-bearing cartilage in the knee. Supplemental acquisitions or reformatting of 3D data sets in the axial and coronal planes may help to optimize evaluation of patellar cartilage and central weight-bearing aspects of the femoral condyles and tibial plateaus, respectively.

Clinical MRI: Cartilage Lesions

Articular cartilage lesions may be categorized as degenerative or traumatic in cause. Early degenerative disease may be seen on MRI as early alterations in cartilage contour morphology (fibrillation, surface irregularity) (Figs. 3A and 3B); changes in cartilage thickness, including cartilage thinning or thickening, which may be an early feature predating cartilage volume loss; or intrachondral alterations in signal intensity potentially related to pre-morphologic intrasubstance collagen degeneration and increased free-water content. Advanced degenerative chondral lesions typically manifest on MRI as multiple areas of cartilage thinning of varying depth and size, usually seen on opposing surfaces of an articulation. Cartilage defects typically illustrate obtuse margins and may be associated with corresponding subchondral regions of increased T2-weighted signal reflective of subchondral edema or cysts or a low signal intensity reflective of subchondral fibrosis or trabecular sclerosis. Other associated MRI findings of degenerative cartilage disease include central and marginal articular osteophytes, joint effusion, and synovitis. In contrast, traumatic chondral lesions generally manifest on routine clinical MRI as solitary focal cartilage defects with acutely angled margins (Figs. 4A and 4B). Traumatic chondral injuries are typically the result of shearing, rotational, or tangential impaction forces and often result in high-grade partial- or full-thickness cartilage tears or in osteochondral injuries of cartilage and the underlying subchondral bone. Linear cartilage clefts or fissures may also be seen, and they can extend for variable depths within the articular cartilage and may result in chondral flap lesions or delamination injuries. Associated alterations in subchondral marrow signal, including bone bruising, bone edema, or subchondral fracture, may be helpful signs in delineating areas of overlying cartilage injury. The finding of a focal signal change in the subchondral bone marrow should encourage careful evaluation of possible overlying hyaline articular cartilage injury or disease. In general, delaminating injuries, superficial flap tears, and surface fibrillation are the most difficult lesions to visualize and assess accurately with MRI. When a traumatic cartilage lesion is identified, its description should include the location, size, and depth of the lesion and the presence or absence of associated chondral fragments. Traumatic cartilage fragments may remain in situ, become partially detached, or become loose and displace into the joint space. As a result, recognition of a traumatic chondral defect should prompt careful inspection of the joint for a displaced intraarticular chondral body.



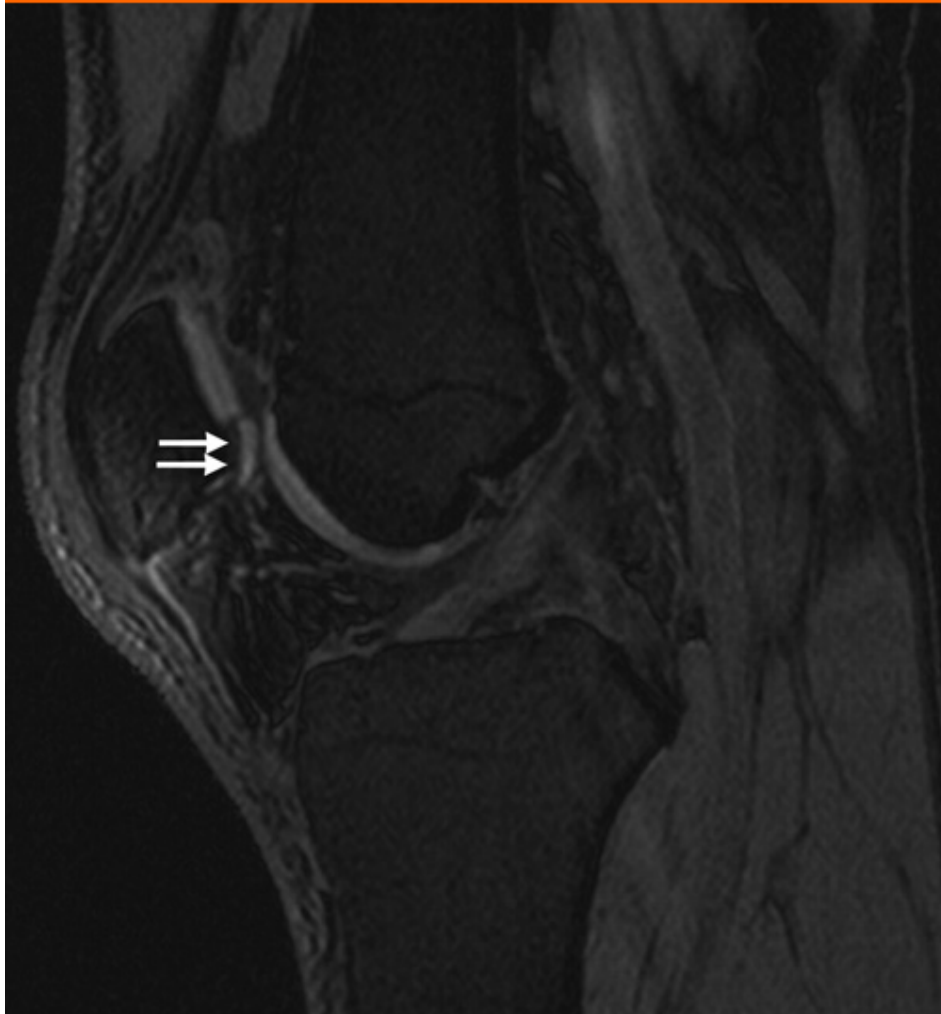


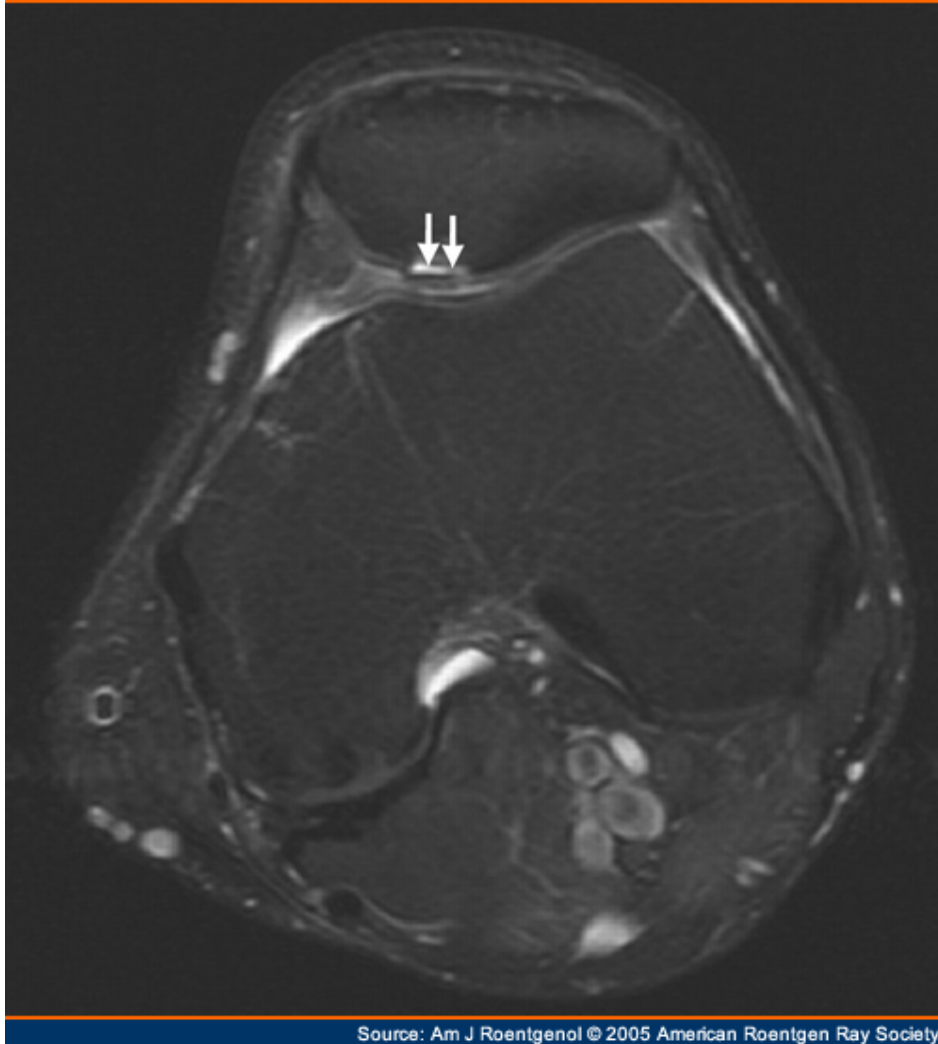
Source: Am J Roentgenol © 2005 American Roentgen Ray Society

Figure 3.

MR images of 61-year-old man with knee pain.

A and **B**, Fat-saturated 3D spoiled gradient-recalled echo image (TR/TE, 50/11; flip angle, 30°) (**A**) and fast spin-echo T2-weighted image (TR/TE, 5,334/91; echo-train length, 4) (**B**) show chondral flap (*arrows*) involving medial femoral condyle.





Source: Am J Roentgenol © 2005 American Roentgen Ray Society

Figure 4.

40-year-old woman with acute knee injury.

A and **B**, Sagittal fat-saturated 3D spoiled gradient-recalled echo image (TR/TE, 22/9; flip angle, 45°) (**A**) and transaxial fast spin-echo image (TR/TE, 3,000/87; echo-train length, 5) (**B**) show chondral fracture (*arrows*) with mild displacement of chondral fragment.

Cartilage Repair Procedures

Articular cartilage itself has limited capability for repair. However, several surgical procedures have been developed to treat cartilage defects. The most common of these procedures can be grouped into two major categories: local stimulation and autologous transplantation of cartilage. Few data exist about how frequently each of these procedures is performed. Because the instrumentation for local stimulation is minimal and the procedure can be performed during arthroscopy, this technique is often performed as the primary repair. Autologous transplantation generally requires exacting surgical techniques and usually is performed by surgeons specializing in it.

Local Stimulation for Cartilage Repair

Several techniques fall into the category of local stimulation, with the three most commonly performed being abrasion arthroplasty, microfracture, and subchondral drilling. All local stimulation techniques rely on formation of a fibrin clot within the defect that is created by bleeding from the penetration of the subchondral bone underlying the chondral lesion. The fibrin clot contains pluripotent stem cells that differentiate and remodel, leading to the formation of repair tissue. The repair tissue has been reported to be fibrocartilage or a hybrid of fibrocartilage and hyaline cartilage.^[58] Although local stimulation techniques are generally recommended for lesions smaller than 4 cm², they have been used to treat defects as large as 10 cm².

Local stimulation techniques differ in the manner in which the subchondral bone is violated. In abrasion arthroplasty, a burr is used to penetrate the bone,^[59] whereas in subchondral drilling, a drill is used to perform this function.^[60] With microfracture, a pick or awl is used to make multiple penetrations into the subchondral bone to about 4 mm in depth and approximately 3-4 mm apart.^[61] Microfracture has been advocated over drilling because less heat and necrosis are thought to occur.

In the first few months after microfracture, MRI shows repair tissue of intermediate signal intensity that is typically thinner than the adjacent native articular cartilage.^[56] Over time, the amount of repair tissue increases, with the optimal result being 100% defect fill with a congruent articular surface and repair tissue of signal intensity similar to that of native articular cartilage (Figs. 5A and 5B). It is common to see an edemalike signal change within the subchondral bone after the procedure, though this change usually resolves over several months.^[56] Failure and complications of microfracture are shown as poor fill of repair tissue and chondral fissures and flaps.





Figure 5.

MR images after microfracture in 32-year-old male professional basketball player. **A** and **B**, Fat-saturated T2-weighted fast spin-echo coronal image (TR/TE, 3,250/90; echo-train length, 5) 2 months after microfracture (**A**) and fat-saturated T2-weighted fast spin-echo image (3,000/85; echo-train length, 5) 7 months after microfracture (**B**) show that repair tissue (*arrows*) is greater at 7 months than at 2 months, with congruent articular surface.

Autologous Transplantation of Cartilage

There are two techniques of autologous transplantation of cartilage: autologous osteochondral transplantation (AOT) and ACI. Both have attracted a great deal of interest because of their potential to form hyaline or hyalinelike repair tissue.

AOT

AOT involves the use of cylindric osteochondral plugs of various sizes to fill chondral defects. The osteochondral plugs are harvested from minimally weight-bearing areas of the joint, typically the periphery of the femoral condyles at the level of the patellofemoral joint. The

plugs vary in diameter from 2.7 to 8.5 mm and in length from 10 to 25 mm.^[58,62] A number of instruments have been developed for performing AOT, leading to several names for this procedure based on the specific instrument used: MosaicPlasty (Acufex, Smith & Nephew), osteochondral autograft transfer system (OATS, Arthrex), soft delivery system (SDS, Sulzermedica), and COR system (Mitek).^[63-70] The chondral defect being repaired is débrided down to viable subchondral bone, and the osteochondral plugs are transplanted into the defect site. The orientation, position, and number of osteochondral plugs are important determinants of the outcome of the procedure. The goal of the procedure is to create a congruent cartilage surface, and the plugs therefore need to be placed perpendicular to the surface. If this placement is not achieved, one edge of the transplant will be raised and one recessed in relation to the native articular cartilage. Both "proud" and recessed plugs have worse outcomes than flush plugs, most likely secondary to abnormal mechanical stress.^[70] By using various sizes of plugs, one can often increase defect fill to 90% or even 100%.^[58] The number of plugs that can be used, however, is limited by the availability of donor sites and the need to limit morbidity at the donor sites. Spaces between plugs fill with a fibrocartilaginous grout, stimulated by abrasion arthroplasty or sharp curettage of the base of the defect. There is often an incongruent bone-bone interface even though there is a congruent cartilage-cartilage interface, because the plugs typically come from a region of the knee joint where the articular cartilage is thinner than at the recipient site.

Indications for autologous autograft transplantation include focal chondral or osteochondral defects, most commonly of the knee but also of other joint surfaces such as the talar dome, humeral capitellum, and femoral head, which have a diameter of 1-4 cm².^[58,62] Larger lesions have been treated, but lesions larger than 8 cm² are contraindicated for treatment because of the limits on the amount of donor cartilage that can be harvested. Contraindications include diffuse cartilage abnormalities such as those seen in inflammatory arthritis, in advanced osteoarthritis, and after septic arthritis and an age greater than 50 years.^[58] Histologic evaluation of autologous osteochondral transplants has shown viable graft hyaline cartilage, with the interstices between graft plugs filled with fibrocartilagelike repair tissue.^[58,67,69]

Theoretic advantages of osteochondral transplantation include the ability to provide a hyaline cartilage repair tissue, the ability to perform the technique with one procedure, the possibility of bone-to-bone healing of the grafts, and the ability to add bone to an osteochondral lesion such as osteochondritis dissecans. Potential disadvantages include the need to use a portion of the articular surface, though not a major weight-bearing surface, as a donor site; the creation of an irregular bone-cartilage interface and possible resultant irregular "tidemark;" and the technical difficulty of the procedure, especially in the accurate placement of the plugs.

MRI after AOT is accurate in evaluating several features of the procedure, including graft positioning, surface congruity, graft incorporation, and donor site morbidity. After the procedure, there should be a congruent cartilage-cartilage interface (Fig. 6). MR images provide excellent visualization of the repair tissue surface and its relationship to adjacent native articular cartilage. When surface irregularity or incongruity is present, MRI can show the reasons for such problems, such as improper positioning of the graft, graft subsidence (Fig. 7), or gross graft motion such as graft displacement or rotation. Surface incongruities, when present, may be seen to decrease over time on serial MRI studies, presumably because of filling of the defects by the fibrocartilaginous grout.^[62]



Source: Am J Roentgenol © 2005 American Roentgen Ray Society

Figure 6.

37-year-old man 2 years after autologous osteochondral transplantation of medial femoral condyle. T2-weighted fast spin-echo coronal image (TR/TE, 6,192/132; echo-train length, 7) shows relatively congruent cartilage surface (*arrows*).



Source: Am J Roentgenol © 2005 American Roentgen Ray Society

Figure 7.

17-year-old boy 3 months after autologous osteochondral transplantation. Fat-saturated 3D spoiled gradient-recalled echo sagittal image (TR/TE, 50/11; flip angle, 40°) shows subsidence of osteochondral plugs (*arrows*), with resultant incongruent articular surface.

The signal characteristics of the cartilage cap on the osteochondral plugs typically follow those of adjacent native articular cartilage. The fibrocartilaginous grout in the spaces between plugs may show increased T2 signal, compared with that of native articular cartilage, on fast spin-echo images and decreased signal intensity, compared with that of adjacent native articular cartilage, on 3D fat-suppressed SPGR sequences.

Animal studies after AOT have shown that graft revascularization begins as early as 6-14 weeks after the procedure.^[71,72] Signal-intensity changes seen on MRI are believed to parallel this process, with the grafts showing a normal, fatlike marrow signal at 2 weeks. By 4-6 weeks, however, an edemalike signal change is seen within the marrow of the graft and in the surrounding bone marrow, with intense enhancement of the graft after IV contrast administration.^[73] The perigraft abnormal signal is believed to represent fibrovascular reparative and inflammatory reactive tissue. Between 6 and 9 months, the graft returns to fatty marrow and enhancement decreases; these changes are thought to be secondary to

incorporation of the graft. Edemalike signal changes in the perigraft tissues also tend to decrease by 1 year after the procedure, though persistence of some edemalike signal change up to 2 years after the procedure has been shown in asymptomatic grafts that appear solidly incorporated on arthroscopy.^[62] However, a large, persistent perigraft edemalike signal change or formation of cystlike regions are worrisome indicators of poor graft incorporation.

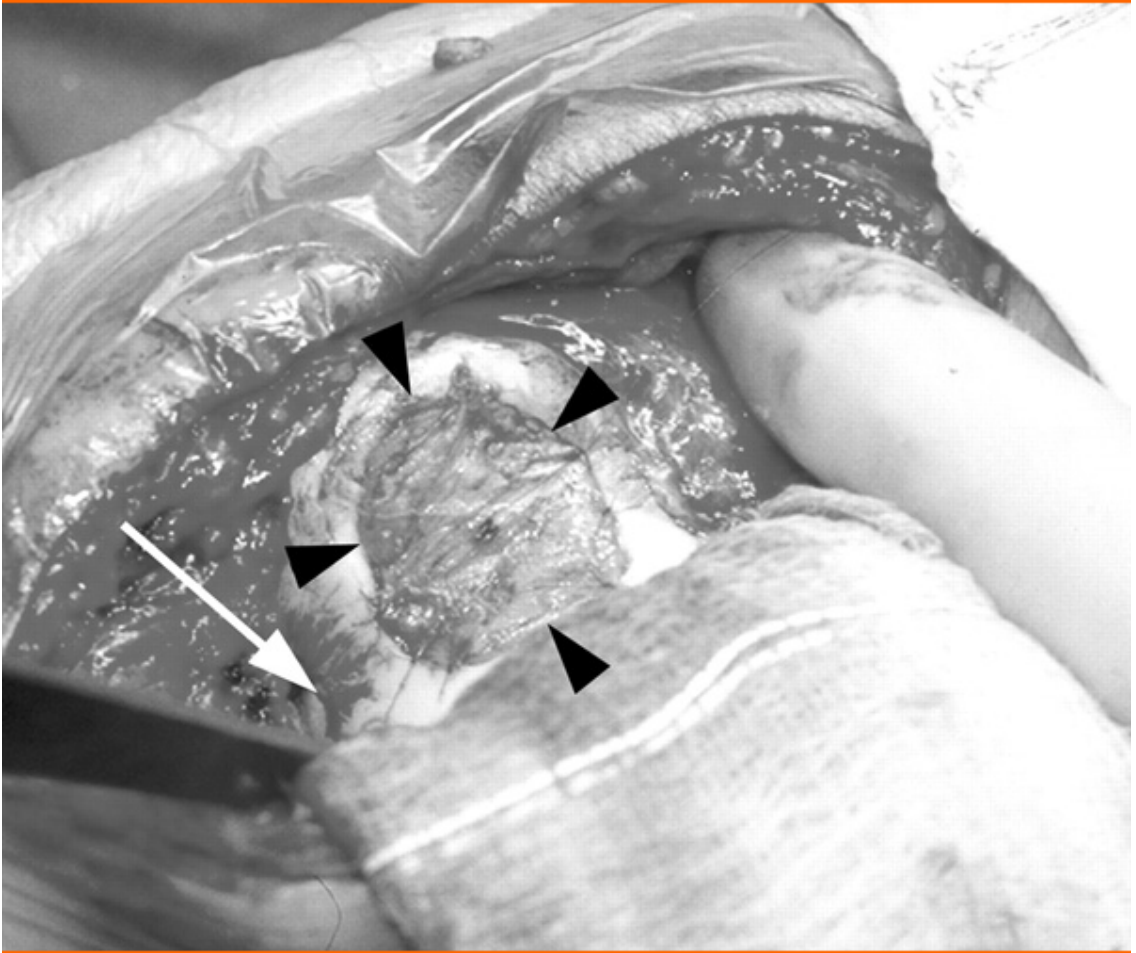
Although the osteochondral plugs are taken from a relatively non-weight-bearing area of the joint, donor site morbidity has been reported in approximately 3% of patients.^[58] After harvesting of the osteochondral plugs, the donor site may be left empty or may be filled with material from the recipient site. Over time, the donor site fills with cancellous bone and fibrocartilagelike material.^[62] In the early postoperative period, the donor sites show low T1 and increased T2 signal intensity, compared with the signal intensity of adjacent fatty marrow, with a defect in the overlying articular cartilage and edemalike signal change in the adjacent bone marrow. Approximately 6-9 months after the procedure, the donor sites return to a fatty, marrowlike signal intensity and the overlying articular cartilage defect fills with fibrocartilagelike repair tissue.

ACI

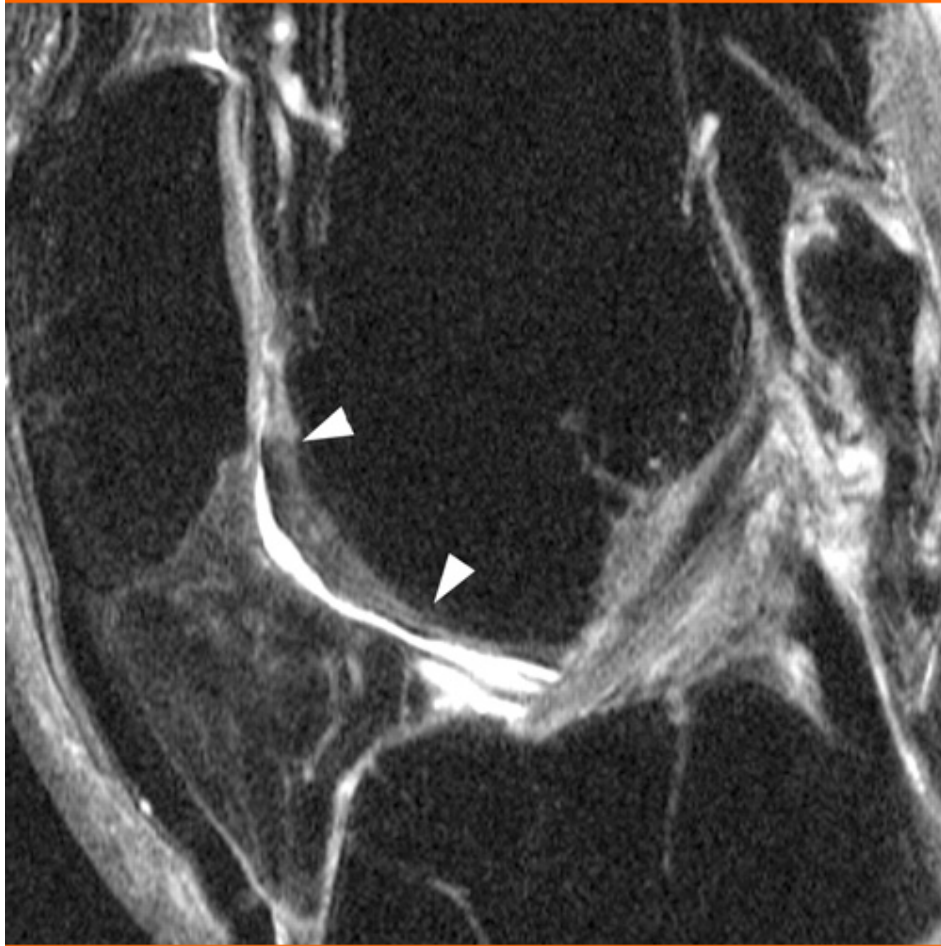
ACI is a cell-based surgical treatment for deep articular cartilage defects.^[74] It has been recommended for defects from 2 to 12 cm² and is performed in two stages. The first stage is an arthroscopic assessment of the cartilage defect and the harvesting of a small amount of articular cartilage from a relatively non-weight-bearing site within the knee, usually the intercondylar notch or the medial margin of the trochlea.^[74,75] The cells within this cartilage biopsy specimen are removed from the extracellular matrix by enzymatic digestion and then cultured for several weeks until approximately 12 million cells are available for implantation.^[76] In the second stage, an open arthrotomy, the repair site is prepared by débridement of the defect by removal of the calcified cartilage layer and any loose cartilage fragments from the margins of the defect. Penetration of the subchondral bone plate is avoided. Periosteum of the same dimensions as the defect is harvested from the tibia or femur. The periosteum is sewn over the prepared defect with the cambium layer facing the bone. Fibrin glue is used to seal the margins of the defect. The cultured cells are then injected beneath the periosteal cover.

The repair site matures through several stages.^[76] During the first 6 weeks, or the proliferative phase, the implanted cells multiply and fill the defect with a very soft tissue. Between weeks 7 and 26, or the transition phase, the extracellular matrix expands and stiffens as collagen and proteoglycans are produced. In the final, or remodeling, phase, the extracellular matrix further matures until the stiffness of the repair tissue becomes similar to that of the adjacent hyaline articular cartilage. Histologic examination of biopsy samples obtained from repairsites showed a hyalinelike repair in 75-80% of cases at a mean follow-up of 4.5 years after ACI.^[77,78]

The normal appearance of the repair site and of the underlying bone after ACI changes as the repair tissue matures.^[56,57,79] During the first month, the tissue within the repair site appears of intermediate signal intensity on unenhanced T1-weighted and proton density-weighted images and of bright signal intensity on T2-weighted and other fluid-sensitive sequences—only slightly different from joint fluid. Images from IV (indirect) arthrograms usually show bright enhancement of the immature repair tissue. During the first several weeks, the periosteal cover may be identified as a separate layer on the surface of the repair site that may extend above the expected level of the articular surface. Over time, the signal intensity of the repair tissue becomes less like fluid and more like native hyaline articular cartilage. After about 12-18 months, the signal intensity of the repair tissue stabilizes. The signal intensity of the mature repair tissue varies and may be quite heterogeneous or only subtly different from adjacent nonoperated articular cartilage (Figs. 8A, 8B, 8C, 8D, and 8E). Most often, the appearance of the repair tissue is different from that of native articular cartilage.^[80] At this time, the implications of the different signal patterns in the repair tissues are not known.











Source: Am J Roentgenol © 2005 American Roentgen Ray Society

Figure 8.

52-year-old man with failed abrasion arthroplasty of medial trochlea who was treated by autologous chondrocyte implantation (ACI). Six years after surgery, he was asymptomatic and underwent imaging with IV (indirect) MRI arthrography.

A, Photograph obtained near end of surgery shows anterior margin of intercondylar notch (*arrow*) and 25-mm-long × 22-mm-wide ACI site (*arrowheads*) covering nearly entire medial trochlear facet.

B, Sagittal proton density-weighted fast spin-echo image (TR/TE, 2,400/37; echo-train length, 8) of knee shows complete fill of trochlear ACI site (*arrowheads*) by repair tissue, which appears slightly darker than native articular cartilage. Levels of articular surface and subchondral bone plate are slightly above those of adjacent, nonoperated regions.

C, Sagittal proton density-weighted fast spin-echo fat-saturated image (2,900/25; echo-train length, 8) of knee shows normal signal in bone marrow subjacent to ACI site (*arrowheads*).

D, Transaxial proton density-weighted fast spin-echo image (3,625/30; echo-train length, 12) of knee shows ACI site (*arrowheads*) on medial trochlear facet filled with low-signal-intensity repair tissue.

E, Oblique coronal T1-weighted spin-echo fat-saturated image (650/12) of knee obtained in plane orthogonal to trochlear ACI site shows area of native articular cartilage thinning (*arrow*) medial to ACI repair site (*arrowheads*). Region of native cartilage thinning is poorly shown on transaxial image (**D**) because of partial-volume artifact.

The repair tissue should restore the contour of the articular surface and fill the cartilage defect to the same level as that of the adjacent articular cartilage, regardless of the depth of the original defect. At the margins of the defect, the repair tissue usually integrates with the adjacent cartilage. This ACI-cartilage interface usually appears as a dark band, or it may be indiscernible. However, during the first few postoperative months, portions of the normal ACI-cartilage interface may appear similar to fluid and simulate a fissure. The fluidlike line in a healthy, immature interface is oriented orthogonally to the articular surface and, unlike a cartilage flap, does not extend between the bone and repair tissue. With time, the normal fluidlike interface matures to become indiscernible or dark, whereas a true fissure persists, with formation of a cartilage flap or subchondral cyst. The subchondral bone plate beneath the repair site usually appears slightly irregular in contour and remains unchanged over time. The bone marrow usually shows intense edemalike signal deep beneath the repair site, often to the level of the physeal scar, during the initial postoperative period. The marrow signal intensity begins to return to normal over the next few months and usually appears nearly normal by 1 year. A thin line of mild edemalike signal may normally remain beneath the subchondral bone plate subjacent to the ACI site indefinitely.

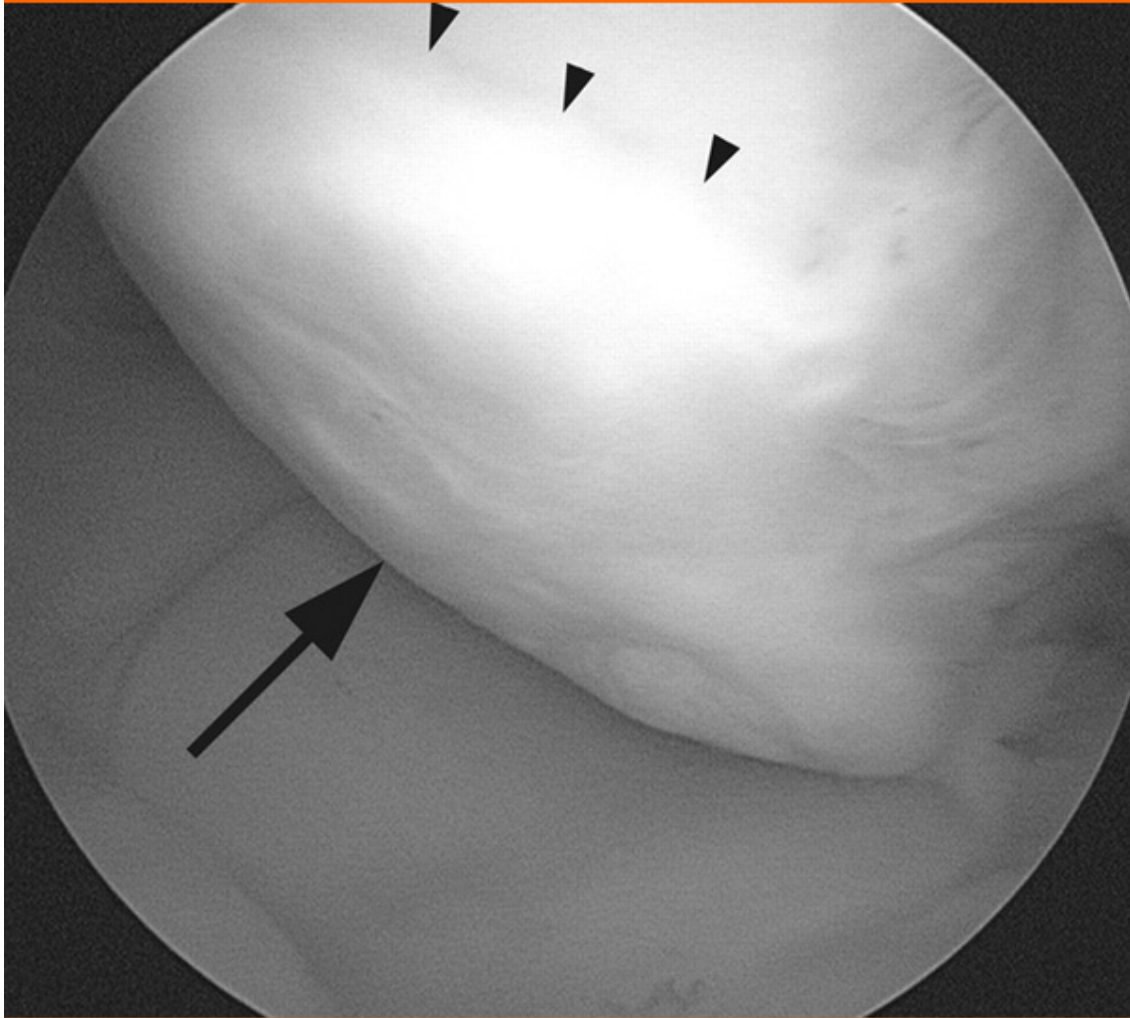
Postoperative complications after ACI are related either to the open arthrotomy or specifically to the ACI graft. Although occurrences in either of these categories may require arthroscopic surgery, they usually they do not indicate treatment failure.^[75,77,78] Most ACI-related complications are associated with the periosteal cover. Failure of the ACI graft through degeneration, fissuring, or separation of the repair tissue from the bone (delamination) is much less common.^[75,77,78]

The formation of intraarticular adhesions causing knee stiffness is the most common arthrotomy-related complication, occurring in about 5% of patients treated with ACI.^[75] Adhesions usually present early, in the first several postoperative months. The diagnosis is most often made without the need for imaging, but the signs and symptoms may be nonspecific. In such cases, MRI may be useful in excluding ACI graft failure and in identifying the thickened fibrous bands of the adhesions. On MR images, postoperative adhesions appear as thickening of the joint capsule or as focal bands of tissue within the infrapatellar fat pad. The signal intensity of the adhesions is usually lower than that of fat on T1-weighted and proton density-weighted images but brighter than that of fat on proton density-weighted images with fat saturation. These bands often extend over the articular cartilage or the ACI repair-tissue surface.

Periosteal complications include fibrous overgrowth of the periosteal cover (periosteal hypertrophy) and separation and detachment of a hypertrophic periosteal cover from the underlying hyaline repair (periosteal delamination). Periosteal hypertrophy is commonly seen at histologic examination and arthroscopy^[75,77] and may be symptomatic in up to 20% of patients.^[75] On MRI, periosteal hypertrophy appears as thickening of the repair tissue, with protrusion of the tissue above the expected level of the articular contour^[57] (Figs. 9A, 9B, and 9C). The hypertrophic tissue may extend over the surface of the adjacent articular cartilage (overlapping type) like a pannus. Or, when the ACI site abuts the intercondylar notch, the hypertrophic tissue may grow into the notch and interfere with the anterior cruciate ligament, similar to the focal fibrosis or "cyclops" lesion seen after anterior cruciate ligament reconstruction.^[57,76] The treatment of symptomatic periosteal hypertrophy is usually by arthroscopic chondroplasty with removal of the overgrown fibrous tissue.^[75]







Source: Am J Roentgenol © 2005 American Roentgen Ray Society

Figure 9.

22-year-old woman with catching sensation in knee 6 months after autologous chondrocyte implantation (ACI) surgery for 24-mm-long × 19-mm-wide osteochondral defect of medial femoral condyle.

A, Sagittal proton density-weighted fast spin-echo image (TR/TE, 2,900/38; echo-train length, 8) of knee from IV (indirect) MR arthrogram shows prominent periosteal hypertrophy. Surface of ACI site (*arrowheads*) is above level of native articular cartilage, best seen at junction between ACI and native cartilage (*arrow*).

B, Sagittal proton density-weighted fast spin-echo fat-saturated image (2,900/25; echo-train length, 8) of knee from same examination as A shows mild edemalike signal in marrow beneath ACI site (*arrowheads*).

C, Image of ACI site from knee arthroscopic surgery performed 19 days after A shows prominent mound of fibrous, periosteal overgrowth (*arrow*) and junction between ACI and native articular cartilage (*arrowheads*). Fibrous periosteal tissue was débrided, revealing firm, intact repair tissue underneath.

Periosteal delamination may result in symptoms of catching or locking of the knee.

Arthroscopic removal of the periosteal cover is usually all that is required, and most often the underlying repair tissue remains intact. The detached fibrous tissue is usually hypertrophic

and lying over the repair site and adjacent articular cartilage and most often appears as a bulge in the articular contour on MR images. Failure of the ACI may occur from poor bone integration, poor repair-tissue quality (soft graft), graft detachment (delamination), or degeneration of the repair tissue.^[75] Clinical failures after ACI have been reported in 6-13% of patients^[75,77,81] Degeneration of the ACI tissue most often presents as pain, years after surgery. On MRI, degeneration of the ACI repair site appears similar to damage of native articular cartilage. Focal full- or partial-thickness defects, fissures, and tissue flaps may be present. The underlying bone often shows intense edemalike marrow signal or cyst formation.^[82]

Delamination of the ACI usually occurs in the first 6 months of the postoperative course.^[76] Delamination may involve all of the graft or only a portion of the graft. When a partial delamination occurs, it usually involves the edge of the ACI where the repair tissue meets the adjacent native articular cartilage.^[76] Symptoms are most commonly the sudden onset of painful catching or knee locking.^[76] The delaminated tissue may become displaced, leaving an empty defect, or remain in situ within the repair site, producing a tissue flap. The MRI appearances of delamination reflect the location of the separated repair tissue.^[57] When the delamination is displaced, the ACI site is empty and fluid-filled. The displaced repair tissue is often found as an intraarticular loose body elsewhere in the joint. On MRI, delamination in situ appears similar to a cartilage flap. A thin, fluidlike signal line is usually seen at the base of the ACI site between the repair tissue and the subjacent subchondral bone plate. Most often, this abnormal linear signal can be seen to connect with the joint space on one or more images. In the first few weeks after surgery, and even in the first 3-4 months, it can be difficult to differentiate the fluidlike signal of the immature ACI repair tissue from joint fluid at the base of the graft from a delamination. MRI arthrography, either direct or indirect, can help because the repair tissue is usually darker than fluid on these acquisitions. However, in some instances, the repair tissue and joint fluid may appear similar even with MRI arthrography.

Assessment of the bone marrow beneath the ACI is an important part of the MRI evaluation. As with other cartilage repair procedures, an edemalike marrow signal subjacent to the repair tissue is a normal finding in the early postoperative period but persistence or reappearance of abnormal marrow signal may indicate problems with the repair.^[57,62,82] The precise time frame for normalization of the marrow signal after ACI has not been established. However, persistence of abnormal marrow signal beyond the first postoperative year is worrisome and may indicate postoperative complications such as periosteal hypertrophy or poor integration of the repair tissue. Subchondral cysts may develop beneath ACI sites, with poor integration of the repair tissue to adjacent cartilage or with degeneration of the repair tissue.^[82]

New Imaging Techniques

Recent medical and surgical advances in the treatment of osteoarthritis and other cartilage abnormalities require improved noninvasive Methods to evaluate articular cartilage. Much research is under way to increase the potential of MRI as a noninvasive method of cartilage analysis, with efforts focused on both qualitative and quantitative analyses. Technologic advances in high-field imaging, pulse sequence development, and the application of MRI contrast agents are the foundation of this work. Imaging articular cartilage is a challenge. It is thin, with a maximum thickness of about 4 mm, and usually has curved surfaces. These factors lead to partial-volume averaging effects, which may reduce the sensitivity of MRI for measurements of cartilage thickness and volume and for the detection of thin fissures, cartilage flaps, and shallow defects. To obtain high-quality MR images, one must maintain a balance between high spatial resolution and adequate SNR. Any increase in the SNR that can be obtained affords the potential to increase the spatial resolution and thus to improve MR image sensitivity for small abnormalities and early disease in articular cartilage. For example, a new MRI system that provides a twofold improvement in SNR should be able to provide a twofold increase in spatial resolution at the same SNR as the old system.

Because SNR is linearly proportional to magnetic field strength, imaging at higher magnetic field strengths should allow greater spatial resolution with equal imaging time and SNR.^[83] If all other factors were to remain equal, a change from a 1.5-T system to a 3-T system, for

instance, should provide a twofold increase in SNR at the same spatial resolution and imaging time, a twofold increase in spatial resolution at the same SNR and imaging time, or a fourfold reduction in imaging time at the same SNR and spatial resolution. However, at higher field strengths, the T1 relaxation times increase, particularly for cartilage. Also, the increase in frequency difference between marrow fat and cartilage water at 3 T versus lower field strength reduces the benefits obtained from an increase in magnet field strength for non-fat-suppressed Methods. Longer T1 relaxation times require longer-pulse TRs, resulting in an increase in image acquisition time or a change in the flip angle of the excitation pulse to maintain the same image contrast at higher field strength.^[83] In addition, for non-fat-suppressed images, the greater separation of fat and water frequencies will lead to greater chemical shift artifacts at the cartilage-bone interface because of marrow fat. Although increasing the bandwidth of the image acquisition may reduce this artifact, the SNR of the acquisition decreases. Despite these challenges, high-field imaging shows great promise as an overall improvement in articular cartilage assessment by MRI. Currently, high-field MRI systems are not as widely available and do not have the same range of radiofrequency coils as are produced for 1.5-T systems. As high-field MRI availability and equipment improve, they will likely become the preferred systems for articular cartilage imaging.

New pulse sequences and image acquisition Methods under development for articular cartilage have focused on image contrast and spatial resolution that would improve both quantitative cartilage analyses and the clinical diagnosis of articular cartilage abnormalities.^[84] A major emphasis of articular cartilage research has been the measurement of articular cartilage thickness and volume as biomarkers for disease progression or treatment response in osteoarthritis.^[85-88] To perform these analyses, it is desirable to use computer algorithms to identify, or "segment," articular cartilage tissue in an automated manner. This goal requires high image contrast between cartilage and the surrounding tissues, including bone, bone marrow, joint fluid, menisci, joint capsule, ligaments, and intraarticular fat. To date, no one acquisition sequence has proven ideal, although the majority of publications on volume and thickness measurements have used the 3D T1-weighted SPGR sequence.^[84,86] Although this sequence shows good cartilage-water and cartilage-fat image contrast, the cartilage-meniscus and cartilage-capsule image contrast has been relatively poor.^[89] A number of other acquisition techniques have been proposed to improve articular cartilage image contrast. These Methods include steady-state free precession (fast imaging employing steady-state acquisition [FIESTA], true fast imaging with steady-state free precession [true-FISP], balanced fast field echo) and its variant, fluctuating equilibrium MRI (FEMR); multi-echo techniques such as dual excitation in the steady state (DESS); driven equilibrium techniques such as driven equilibrium Fourier transform (DEFT) and fast recovery fast spin echo; echo-planar techniques such as 3D echo-planar imaging with fat suppression and 3D DEFT; and 3D fast spin-echo Methods^[90-96] (Figs. 10A and 10B). Automated and semiautomated image-processing approaches that combine two image acquisitions—for example, subtraction of image acquisitions with and without binomial pulse saturation transfer—have shown the ability to isolate articular cartilage automatically for volume and thickness measurements.^[97] However, double-acquisition techniques can be time-consuming and may require image registration if the patient moves between acquisitions.

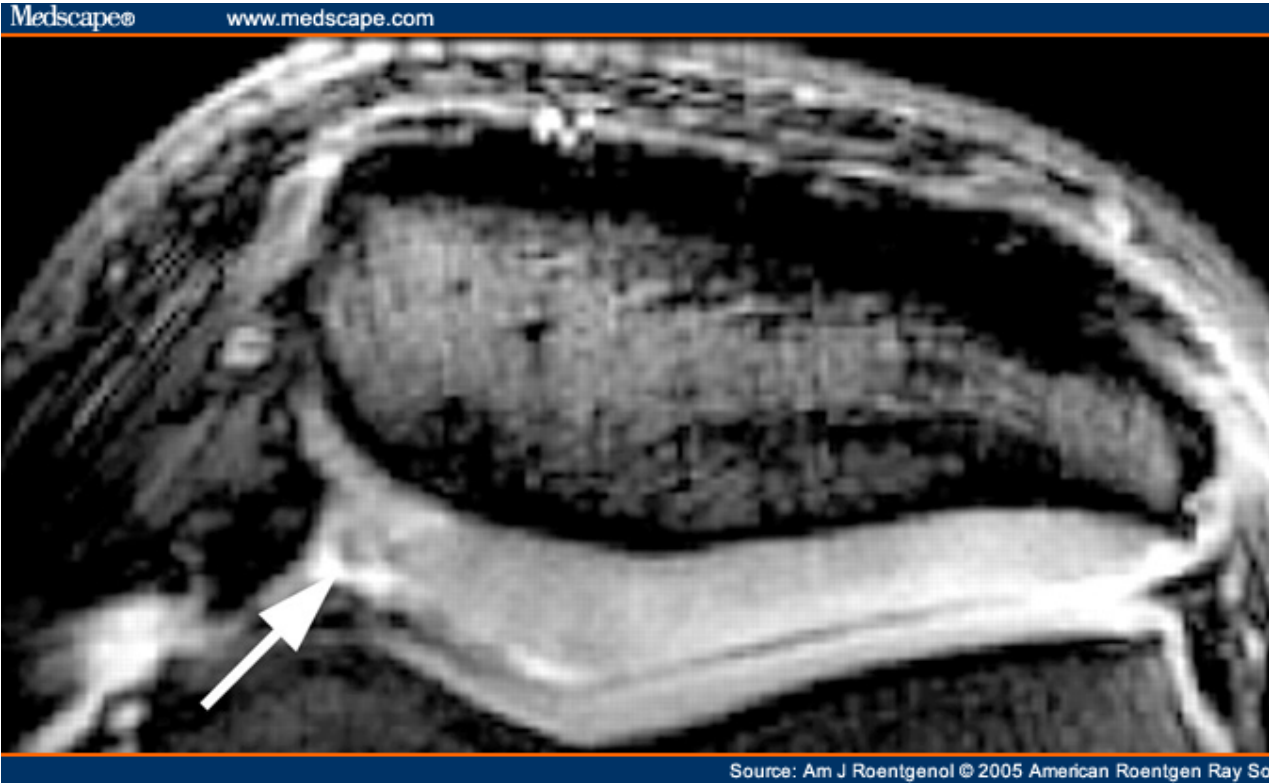


Figure 10.

Transaxial MR images of patellofemoral joint of patient with knee pain. (Reprinted with permission from^[90])

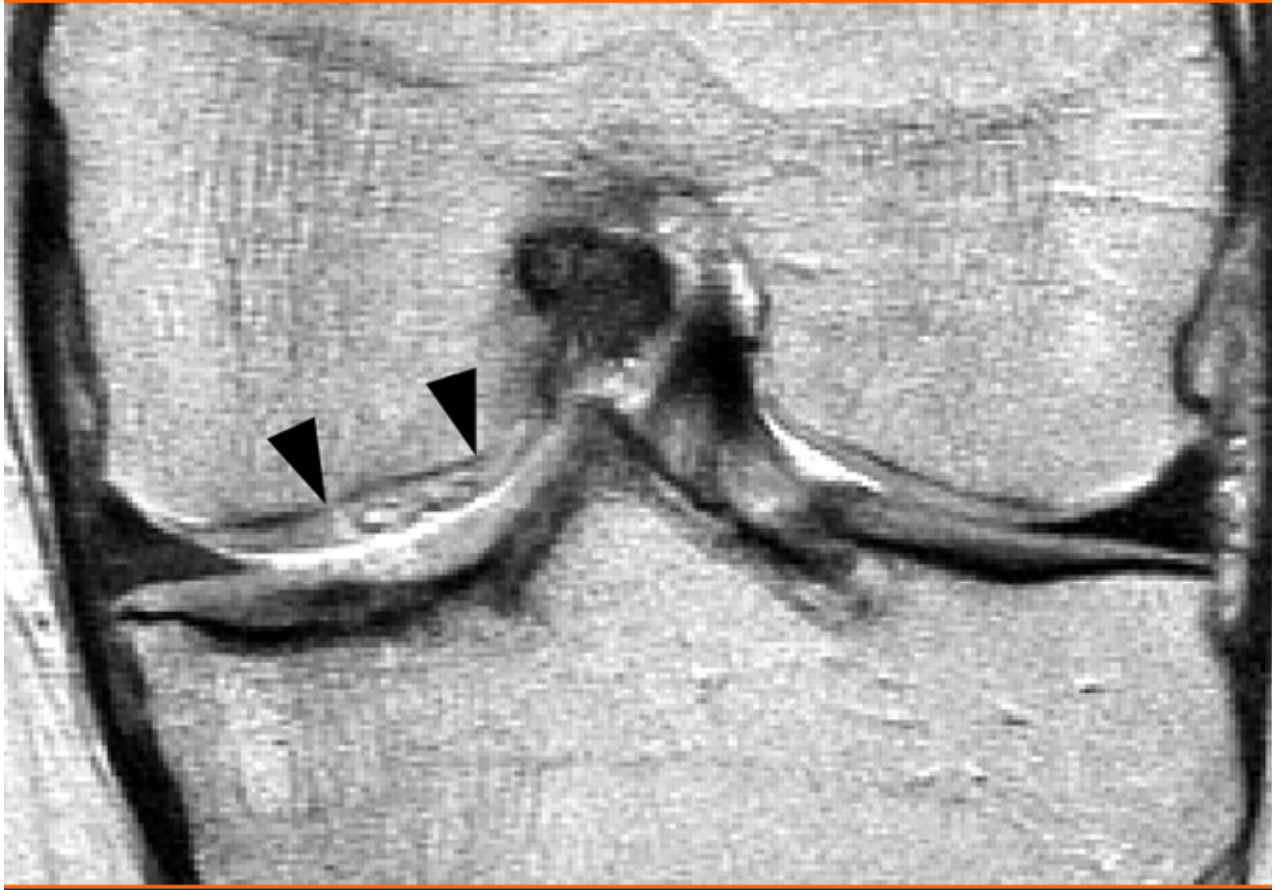
A, Driven equilibrium Fourier transform (DEFT) image with fat saturation (TR/TE, 400/15)

clearly shows deep cartilage fissure with surface irregularity (*arrow*).

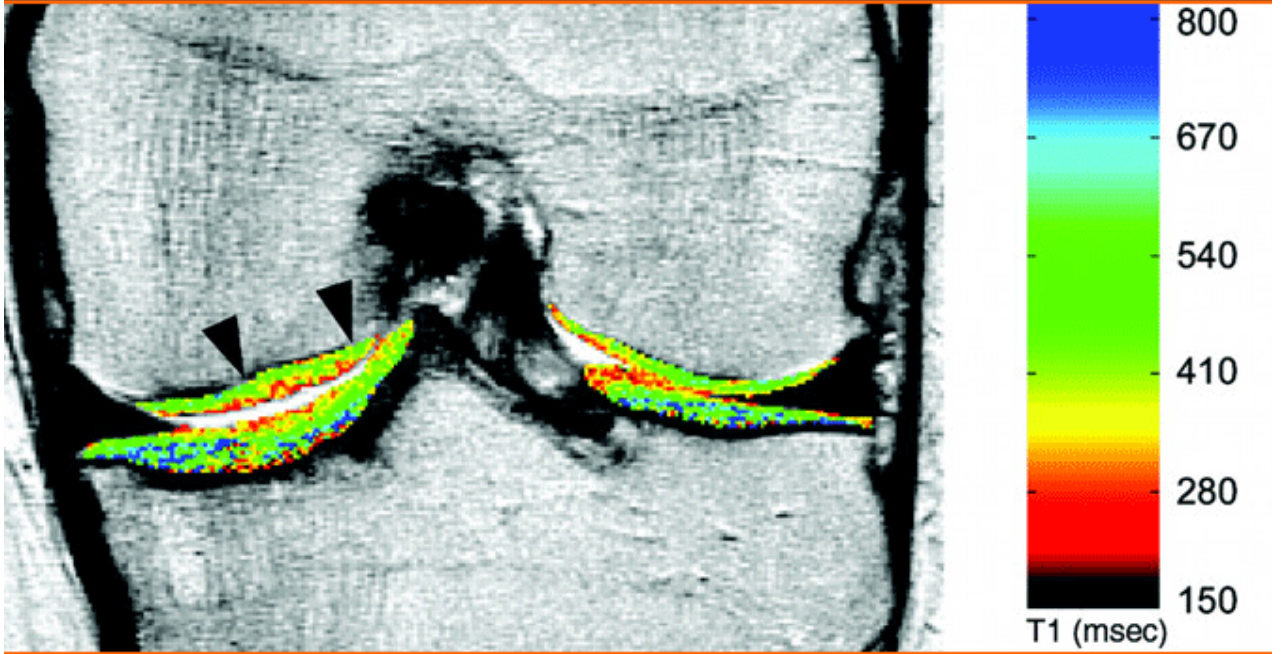
B, On spoiled gradient-recalled echo fat-saturated image (50/15; flip angle, 30°) obtained at same location, abnormality is more difficult to visualize (*arrow*).

Improvements in spatial resolution have been achieved by the use of 3D acquisition techniques with thinner slices to produce isotropic voxels.^[96] Imaging at a high field strength may be required to achieve an adequate SNR, and the longer acquisition times with isotropic acquisitions risk compromise of the studies by patient motion. The advantages of acquiring voxels with equal dimensions in three planes include the ability to reformat the image data in any plane without a loss of spatial resolution and a potential improvement in the diagnosis and quantitative measurement of cartilage abnormalities because of the reduction in partial-volume artifacts. A number of imaging pulse sequences have shown sensitivity to changes in specific structural and biochemical components of articular cartilage. For example, measurement of T2 relaxation times and visualization of focal changes in the T2 relaxation times observed in symptomatic patients may be related to local damage to collagen.^[9,22,52] Magnetization transfer, T1-rho, and sodium content through sodium-23 imaging have been investigated as potential measures of local collagen and proteoglycan concentrations within cartilage.^[41,98-101] Diffusion of water within articular cartilage should relate to the biochemical content of the extracellular matrix and has been investigated as a potential measure of cartilage degradation.^[102,103] Most imaging sequences are affected by changes in more than one of the cartilage components, and degeneration of cartilage is a complex combination of structural and biochemical changes. More research in this area will be required to develop a quantitative noninvasive measure of early cartilage abnormalities that is sensitive for progression of disease.

A contrast agent-based MRI technique, delayed gadolinium-enhanced MR imaging of cartilage (dGEMRIC), measures glycosaminoglycan content within cartilage.^[104,105] This technique takes advantage of the repulsive electrostatic interaction between the negative charges on glycosaminoglycans and the negative charges on Gd-DTPA²⁻ (gadolinium diethylenetriamine pentacetic acid) to measure the distribution of glycosaminoglycan within cartilage. At equilibrium, the local amount of Gd-DTPA²⁻ within the cartilage matrix is inversely proportional to the local concentration of glycosaminoglycan. Normal regions of cartilage have a low Gd-DTPA²⁻ concentration, whereas abnormal regions of cartilage have relatively high concentrations. The technique is performed by IV injection of a double dose of gadopentetate dimeglumine (0.2 mmol/L per kilogram) followed by an approximately 2-hr delay for equilibration of the contrast agent within the cartilage.^[106] T1 measurements are then performed, and the images are used to calculate T1 maps that reflect the local distribution of Gd-DTPA²⁻. On these T1 maps, areas of low T1 represent regions of low glycosaminoglycan (high concentration of Gd-DTPA²⁻) (Figs. 11A and 11B). dGEMRIC holds great promise to measure biochemical changes within morphologically intact cartilage that may reflect early cartilage degeneration or maturation of cartilage repair tissue.^[99,107-109]



Source: Am J Roentgenol © 2005 American Roentgen Ray Society



Source: Am J Roentgenol © 2005 American Roentgen Ray Society

Figure 11.

MR images from delayed gadolinium-enhanced MR imaging of cartilage study of knee of 41-year-old man after treatment of cartilage defect of medial femoral condyle with autologous chondrocyte implantation (ACI).

A, Coronal STIR fast spin-echo MR image (TR/TE, 1,800/14; inversion time, 1,650 msec; echo-train length, 7) of knee obtained 2 hr after IV injection of 0.2 mmol of gadopentetate dimeglumine per kilogram of body weight shows complete fill of ACI site (*arrowheads*) on medial femoral condyle. Surface of repair site is slightly irregular. Signal intensity of superficial layer of articular cartilage of medial tibial plateau appears mildly frayed.

B, Color-encoded T1 map of cartilage obtained from set of 7 STIR images with inversion times ranging from 50 to 1,650 msec is superimposed on gray-scale image of knee. T1 value of repair tissue (*arrowheads*) in ACI site is 83% of that of adjacent, native articular cartilage of medial femoral condyle, indicating slightly lower concentration of glycosaminoglycans within repair tissue. Lower T1 values within superficial articular cartilage of medial femoral condyle and tibial plateaus indicate loss of glycosaminoglycans.

Other contrast agents under investigation include dendrimer-linked nitroxides and liposome-containing compounds. Preliminary studies have shown that stable nitroxides that are positively charged or linked to positively charged dendrimers are preferentially taken up by cartilage when injected into the joint.^[110,111] This new family of MRI contrast agents has a variety of molecular sizes and net molecular charges that may prove useful in probing the structure of articular cartilage. A second approach involves the incorporation of MRI contrast agents into liposomes.^[112,113] By encapsulation within the liposomes, the contrast agent is excluded from cartilage by an intact surface layer. Areas of abnormal cartilage degraded by collagenase could be detected, presumably because the liposomes could enter into the larger spaces created by the collagen degradation.^[113]

Summary

Over the past decade, MRI of articular cartilage has become one of the leading areas of clinical and research interest. The development of cartilage-specific sequences has made MRI the optimal technique for the evaluation of cartilage abnormalities and repair procedures. In addition, this intense focus has produced numerous innovations allowing the investigation of the structural and biochemical changes that occur with cartilage degeneration and injury.

References

1. Recht MP, Resnick D. MR imaging of articular cartilage: current status and future directions. *AJR* 1994;163 : 283-290
2. Xia Y, Farquhar T, Burton-Wurster N, Lust G. Origin of cartilage laminae in MRI. *J Magn Reson Imaging* 1997; 7:887 -894
3. Lehner KB, Rechl HP, Gmeinwieser JK, Heuck AF, Lukas HP, Kohl HP. Structure, function, and degeneration of bovine hyaline cartilage: assessment with MR imaging in vitro. *Radiology* 1989;170 : 495-499
4. Rubenstein JD, Kim JK, Henkelman RM. Effects of compression and recovery on bovine articular cartilage: appearance on MR images. *Radiology* 1996;201 : 843-850
5. Mlynarik V, Degrassi A, Toffanin R, Vittur F, Cova M, Pozzi-Mucelli RS. Investigation of laminar appearance of articular cartilage by means of magnetic resonance microscopy. *J Magn Reson Imaging* 1996; 14:435 -442
6. Frank L, Brossmann J, Buxton R, Resnick D. MR imaging truncation artifacts can create a false laminar appearance in cartilage. *AJR* 1997; 168:547 -554
7. Mlynarik V, Degrassi A, Toffanin R, Jarh O, Vittur F. A method of generating magnetic resonance microimaging T2 maps with low sensitivity to diffusion. *Magn Reson Med* 1996;35 : 423-425
8. Xia Y. Relaxation anisotropy in cartilage by NMR microscopy (muMRI) at 14-micron resolution. *Magn Reson Med* 1998; 39:941 -949

9. Brossmann J, Frank LR, Pauly JM, et al. Short echo time projection reconstruction MR imaging of cartilage: comparison with fat-suppressed spoiled GRASS and magnetization transfer contrast MR imaging. *Radiology* 1997;203 : 501-507
10. Rand T, Imhof H, Czerny C, et al. Discrimination between fluid, synovium, and cartilage in patients with rheumatoid arthritis: contrast enhanced spin echo versus non-contrast-enhanced fat-suppressed gradient echo MR imaging. *Clin Radiol* 1999;54 : 107-110
11. Recht MP, Kramer J, Marcelis S, et al. Abnormalities of articular cartilage in the knee: analysis of available MR techniques. *Radiology* 1993;187 : 473-478
12. Erickson SJ, Waldschmidt JG, Czervionke LF, Prost RW. Hyaline cartilage: truncation artifact as a cause of trilaminar appearance with fat-suppressed three-dimensional spoiled gradient-recalled sequences. *Radiology* 1996;201 : 260-264
13. Yao L, Gentili A, Thomas A. Incidental magnetization transfer contrast in fast spin-echo imaging of cartilage. *J Magn Reson Imaging* 1996; 6:180 -184
14. Akeson WH, Amiel D, Gershuni DH. Articular cartilage physiology and metabolism. In: Resnick D, ed. *Diagnosis of bone and joint disorders*, 3rd ed. Philadelphia, PA: Saunders, 1995:769 -790
15. Mow VC, Fithian DC, Kelly M. Fundamentals of articular cartilage and meniscus biomechanics. In: Ewing JW, ed. *Articular cartilage and knee joint function*. New York, NY: Raven Press, 1990 : 1-18
16. Rubenstein JD, Kim JK, Morova-Protzner I, Stanchev PL, Henkelman RM. Effects of collagen orientation on MR imaging characteristics of bovine articular cartilage. *Radiology* 1993;188 : 219-226
17. Fullerton GD, Cameron IL, Ord VA. Orientation of tendons in the magnetic field and its effect on T2 relaxation times. *Radiology* 1985;155 : 433-435
18. Henkelman RM, Stanisz GJ, Kim JK, Bronskill MJ. Anisotropy of NMR properties of tissues. *Magn Reson Med* 1994; 32:592 -601
19. Mlynarik V, Trattnig S. Physicochemical properties of normal articular cartilage and its MR appearance. *Invest Radiol* 2000; 35:589 -594
20. Grunder W, Wagner M, Werner A. MR-microscopic visualization of anisotropic internal cartilage structures using the magic angle technique. *Magn Reson Med* 1998;39 : 376-382
21. Goodwin DW, Zhu H, Dunn JF. In vivo MR imaging of hyaline cartilage: correlation with scanning electron microscopy. *AJR* 2000; 174:405 -409
22. Kaab MJ, Gwynn IA, Notzli HP. Collagen fibre arrangement in the tibial plateau articular cartilage of man and other mammalian species. *J Anat* 1998; 193:23 -34
23. Jeffery AK, Blunn GW, Archer CW, Bentley G. Three-dimensional collagen architecture in bovine articular cartilage. *J Bone Joint Surg Br* 1991; 73:795 -801
24. Clark JM. Variation of collagen fiber alignment in a joint surface: a scanning electron microscope study of the tibial plateau in dog, rabbit, and man. *J Orthop Res* 1991;9 : 246-257
25. Clark JM, Simonian PT. Scanning electron microscopy of "fibrillated" and "malacic" human articular cartilage: technical considerations. *Microsc Res Tech* 1997; 37:299 -313
26. Goodwin DW, Dunn JF. High-resolution magnetic resonance imaging of articular cartilage: correlation with histology and pathology. *Top Magn Reson Imaging* 1998; 9:337 -347
27. Goodwin DW. Visualization of the macroscopic structure of hyaline cartilage with MR imaging. *Semin Musculoskelet Radiol* 2001; 5:305 -312
28. Hultkrantz W. *Uber Die Spaltrichtungen Der Gelenkknorpel*. *Verh Anat Ges* 1898;12 : 248
29. Meachim G, Denham D, Emery IH, Wilkinson PH. Collagen alignments and artificial splits at the surface of human articular cartilage. *J Anat* 1974; 118:101 -118
30. Goodwin DW, Ziam Wadghiri Y, Zhu H, Vinton CJ, Smith ED, Dunn JF. The macroscopic structure of tibial plateau articular cartilage: influence of a characteristic matrix architecture on MRIs. *AJR* 2004; 182:311 -318
31. Mosher TJ, Smith H, Dardzinski BJ, Schmithorst VJ, Smith MB. MR imaging and T2 mapping of femoral cartilage: in vivo determination of the magic angle effect. *AJR* 2001;177 : 665-669

32. Goodwin DW, Dunn JF. MR imaging and T2 mapping of femoral cartilage. *AJR* 2002;178 : 1568-1569
33. Totterman S, Weiss SJ, Szumowski J, et al. MR fat suppression technique in the evaluation of normal structures of the knee. *J Comput Assist Tomogr* 1989;13 : 473-478
34. Chandnani VP, Ho C, Chu P, Trudell D, Resnick D. Knee hyaline articular cartilage evaluated with MR imaging: a cadaveric study involving multiple imaging sequences and intraarticular injection of gadolinium and saline solution. *Radiology* 1991;178 : 557-561
35. Konig H, Sauter R, Deimling M, Vogt M. Cartilage disorders: comparison of spin-echo, CHESSE, and FLASH sequence MR images. *Radiology* 1987;164 : 753-758
36. Recht MP, Piraino DW, Paletta GA, Schils JP, Belhobek GH. Accuracy of fat-suppressed three-dimensional spoiled gradient-echo FLASH MR imaging in the detection of patellofemoral articular cartilage abnormalities. *Radiology* 1996;198 : 209-212
37. Disler DG, Peters TL, Muscoreil SJ, et al. Fat-suppressed spoiled GRASS imaging of knee hyaline cartilage: technique optimization and comparison with conventional MR imaging. *AJR* 1994;163 : 887-892
38. Disler DG, McCauley TR, Wirth CR, Fuchs MD. Detection of knee hyaline cartilage defects using fat-suppressed three-dimensional spoiled gradient-recalled echo MR imaging: comparison with standard MR imaging and correlation with arthroscopy. *AJR* 1995;165 : 377-382
39. Disler DG, McCauley TR, Kelman CG, et al. Fat-suppressed three-dimensional spoiled gradient-echo MR imaging of hyaline cartilage defects in the knee: comparison with standard MR imaging and arthroscopy. *AJR* 1996; 167:127 -132
40. McCauley TR, Disler DG. MR imaging of articular cartilage. *Radiology* 1998;209 : 629-640
41. Hardy PA, Recht MP, Piraino DW. Fat suppressed MRI of articular cartilage with a spatial-spectral excitation pulse. *J Magn Reson Imaging* 1998; 8:1279 -1287
42. Gray ML, Burstein D, Lesperance LM, Gehrke L. Magnetization transfer in cartilage and its constituent macromolecules. *Magn Reson Med* 1995; 34:319 -325
43. Wolff SD, Chesnick S, Frank JA, Lim KO, Balaban RS. Magnetization transfer contrast: MR imaging of the knee. *Radiology* 1991; 179:623 -628
44. Potter HG, Linklater JM, Allen AA, Hannafin JA, Haas SB. Magnetic resonance imaging of articular cartilage in the knee: an evaluation with use of fast spin-echo imaging. *J Bone Joint Surg Am* 1998; 80:1276 -1284
45. Broderick LS, Turner DA, Renfrew DL, Schnitzer TJ, Huff JP, Harris C. Severity of articular cartilage abnormality in patients with osteoarthritis: evaluation with fast spin-echo MR vs arthroscopy. *AJR* 1994; 162:99 -103
46. Bredella MA, Triman PFJ, Peterfy CG, et al. Accuracy of T2-weighted fast spin-echo MR imaging with fat saturation in detecting cartilage defects in the knee: comparison with arthroscopy in 130 patients. *AJR* 1999; 172:1073 -1080
47. Sonin AH, Pensy RA, Mulligan ME, Hatem S. Grading articular cartilage of the knee using fast spin-echo proton density-weighted MR imaging without fat suppression. *AJR* 2002;179 : 1159-1166
48. Mohr A. The value of water-excitation 3D FLASH and fat-saturated PDw TSE MR imaging for detecting and grading articular cartilage lesions of the knee. *Skeletal Radiol* 2003;32 : 396-402
49. McCauley TR, Kier R, Lynch KJ, Jokl P. Chondromalacia patellae: diagnosis with MR imaging. *AJR* 1992;158 : 101-105
50. De Smet AA, Monu JU, Fisher DR, Keene JS, Graf BK. Signs of patellar chondromalacia on sagittal T2-weighted magnetic resonance imaging. *Skeletal Radiol* 1992;21 : 103-105
51. Dardzinski BJ, Mosher TJ, Li S, Van Slyke MA, Smith MB. Spatial variation of T2 in human articular cartilage. *Radiology* 1997;205 : 546-550
52. Mosher TJ, Dardzinski BJ, Smith MB. Human articular cartilage: influence of aging and early symptomatic degeneration on the spatial variation of T2—preliminary findings at 3T. *Radiology* 2000; 214:259 -266

53. Cheung LP, Li KC, Hollett MD, Bergman AG, Herfkens RJ. Meniscal tears of the knee: accuracy of detection with fast spin-echo MR imaging and arthroscopic correlation in 293 patients. *Radiology*1997; 203:508 -512
54. Ha TP, Li KC, Beaulieu CF, et al. Anterior cruciate ligament injury: fast spin-echo MR imaging with arthroscopic correlation in 217 examinations. *AJR* 1998;170 : 1215-1219
55. Kapelov SR, Teresi LM, Bradely WG, et al. Bone contusions of the knee: increased lesion detection with fast spin-echo MR imaging with spectroscopic fat saturation. *Radiology*1993; 189:901 -904
56. Alparslan L, Winalski CS, Boutin RD, Minas T. Postoperative magnetic resonance imaging of articular cartilage repair. *Semin Musculoskel Radiol* 2001; 5:345 -363
57. Alparslan L, Minas T, Winalski CS. Magnetic resonance imaging of autologous chondrocyte implantation. *Semin Ultrasound CT MR* 2001; 22:341 -351
58. Hangody L, Rathonyi GK, Duska Z, Vasarhelyi G, Fules P, Modis L. Autologous osteochondral mosaicplasty: surgical technique. *J Bone Joint Surg Am* 2004; 86[suppl 1]: 65-72
59. Buckwalter JA, Mow VC. Cartilage repair in osteoarthritis. In: Moskowitz RW, Howell DS, Goldberg VM, Mankin HJ, eds. *Osteoarthritis, diagnosis and medical/surgical management*, 2nd ed. Philadelphia, PA: Saunders, 1992:71 -107
60. Pridie KH, Gordon G. A method of resurfacing osteoarthritic knee joints. *J Bone Joint Surgery Br* 1959;41 : 618-619
61. Steadman J, Rodkey W, Singleton S, Briggs K. Microfracture technique for full-thickness chondral defects: technique and clinical Results. *Oper Tech Orthop* 1997;7 : 300-304
62. Recht M, White LM, Winalski C, et al. MR imaging of cartilage repair procedures. *Skeletal Radiol* 2003;32 : 185-200
63. Berlet GC, Mascia A, Miniaci A. Treatment of unstable osteochondritis dessicans lesions of the knee using autogenous osteochondral grafts (mosaicplasty). *Arthroscopy* 1999;15 : 312-316
64. Bobic V. Arthroscopic osteochondral autograft transplantation in anterior cruciate ligament reconstruction: a preliminary clinical study. *Knee Surg Sports Traumatol Arthrosc* 1996;3 : 318-321
65. Hangody L, Feczko P, Bartha L, Bodo G, Kish G. Mosaicplasty for treatment of articular defects of the knee and ankle. *Clin Orthop* 2001; 319:328 -336
66. Hangody L, Kish G, Karpati Z, et al. Mosaicplasty for the treatment of articular cartilage defects: application in clinical practice. *Orthopedics* 1998;21 : 751-756
67. Hangody L, Kish G, Karpati Z, Eberhardt R. Osteochondral plugs: autogenous osteochondral mosaicplasty for the treatment of focal chondral and osteochondral articular defects. *Oper Tech Orthop*1997; 7:312 -322
68. Kish G, Modis L, Hangody L. Osteochondral mosaicplasty for the treatment of focal chondral and osteochondral lesions of the knee and talus in the athlete: rationale, indications, techniques and Results. *Clin Sports Med* 1999; 18:45 -66
69. Pearce SG, Hurtig MB, Clarnette R, Kalra M, Cowan B, Miniaci A. An investigation of 2 techniques for optimizing joint surface congruency using multiple cylindrical osteochondral autografts. *Arthroscopy* 2001;17 : 50-55
70. Duchow J, Hess T, Kohn D. Primary stability of press-fit-implanted osteochondral grafts: influence of graft size, repeated insertion, and harvesting technique. *Am J Sports Med*2000; 28:24 -27
71. Dew TI, Martin RA. Functional, radiographic, and histologic assessment of healing of autogenous osteochondral grafts and full thickness cartilage defects in the talus of dogs. *Am J Vet Res*1992; 53:2141 -2152
72. Lane JM, Brighton CT, Ottens HR, Lipton M. Joint resurfacing in the rabbit using autologous osteochondral graft. *J Bone Joint Surg Am* 1977; 59:218 -222
73. Sanders TG, Mentzer KD, Miller M, Morrison WB, Campbell SE, Penrod BJ. Autogenous osteochondral "plug" transfer for the treatment of focal chondral defects: postoperative MR appearance with clinical correlation. *Skeletal Radiol* 2001;30 : 570-578
74. Brittberg M, Lindahl A, Nilsson A, Ohlsson C, Isaksson O, Peterson L. Treatment of deep cartilage defects in the knee with autologous chondrocyte transplantation. *N Engl J Med* 1994;331 : 889-895

75. Minas T. Autologous chondrocyte implantation for focal chondral defects of the knee. *Clin Orthop* 2001;391S : 349-361
76. Minas T, Peterson L. Advanced techniques in autologous chondrocyte transplantation. *Clin Sports Med* 1999;18 : 13-44
77. Peterson L, Minas T, Brittberg M, Nilsson A, Sjogren-Jansson E, Lindahl A. Two- to 9-year outcome after autologous chondrocyte transplantation of the knee. *Clin Orthop* 2000;374 : 212-234
78. Peterson L, Brittberg M, Kiviranta I, Akerlund EL, Lindahl A. Autologous chondrocyte transplantation: biomechanics and long-term durability. *Am J Sports Med* 2002;30 : 2-12
79. Burkart A, Imhoff AB. Diagnostic imaging after autologous chondrocyte transplantation: correlation of magnetic resonance tomography, histological and arthroscopic findings [in German]. *Orthopade* 2000;29 : 135-144
80. Roberts S, McCall IW, Darby AJ, et al. Autologous chondrocyte implantation for cartilage repair: monitoring its success by magnetic resonance imaging and histology. *Arthritis Res Ther* 2003; 5:R60 -R73
81. Micheli LJ, Browne JE, Erggelet C, et al. Autologous chondrocyte implantation of the knee: multicenter experience and minimum 3-year follow-up. *Clin J Sports Med* 2001;11 : 223-228
82. Azer N, Winalski CS, Minas T. Magnetic resonance imaging for surgical planning and postoperative assessment in early osteoarthritis. *Radiol Clin North Am* 2004;42 : 43-60
83. Takahashi M, Uematsu H, Hatabu H. MR imaging at high magnetic fields. *Eur J Radiol* 2003;46 : 45-52
84. Gold GE, McCauley TR, Gray ML, Disler DG. What's new in cartilage? *RadioGraphics* 2003;23 : 1227-1242
85. Solloway S, Hutchinson CE, Waterton JC, Taylor CJ. The use of active shape models for making thickness measurements of articular cartilage from MR images. *Magn Reson Med* 1997;37 : 943-952
86. Eckstein F, Schnier M, Haubner M, et al. Accuracy of cartilage volume and thickness measurements with magnetic resonance imaging. *Clin Orthop* 1998;352 : 137-148
87. Stammberger T, Eckstein F, Michaelis M, Englmeier KH, Reiser M. Interobserver reproducibility of quantitative cartilage measurements: comparison of B-spline snakes and manual segmentation. *Magn Reson Imaging* 1999; 17:1033 -1042
88. Warfield SK, Kaus M, Jolesz FA, Kikinis R. Adaptive, template moderated, spatially varying statistical classification. *Med Image Anal* 2000; 4:43 -55
89. Yoshioka H, Stevens K, Genovese M, Dillingham MF, Lang P. MRI of articular cartilage of the knee: normal patterns mimicking pathology in normal subjects and patients with osteoarthritis. *Radiology* 2004; 231:31 -38
90. Hargreaves BA, Gold GE, Lang PK, et al. MR imaging of articular cartilage using driven equilibrium. *Magn Reson Med* 1999; 42:695 -703
91. Hargreaves BA, Gold GE, Beaulieu CF, Vasanaawala SS, Nishimura DG, Pauly JM. Comparison of new sequences for high-resolution cartilage imaging. *Magn Reson Med* 2003;49 : 700-709
92. Ba-Ssalamah A, Schibany N, Puig S, Herneth AM, Noebauer-Huhmann IM, Trattnig S. Imaging articular cartilage defects in the ankle joint with 3D fat-suppressed echo planar imaging: comparison with conventional 3D fat-suppressed gradient echo imaging. *J Magn Reson Imaging* 2002; 16:209 -216
93. Vasanaawala SS, Pauly JM, Nishimura DG, Gold GE. MR imaging of knee cartilage with FEMR. *Skeletal Radiol* 2002; 31:574 -580
94. Reeder SB, Pelc NJ, Alley MT, Gold GE. Rapid MR imaging of articular cartilage with steady-state free precession and multipoint fat-water separation. *AJR* 2003;180 : 357-362
95. Menick BJ, Bobman SA, Listerud J, Atlas SW. Thin-section, three-dimensional Fourier transform, steady-state free precession MR imaging of the brain. *Radiology* 1992;183 : 369-377
96. Lang P, Zhao L, Zou K, Winalski C, Warfield S, Jolesz FA. Cartilage imaging at 3.0T: comparison of standard 3D SPGR with 3D spectral spatial SPGR and 3D FSE sequences. Presented at 89th Scientific Assembly and Annual Meeting of the Radiological Society of North America; 2003; Chicago, IL

97. Peterfy CG, Van Dijke CF, Janzen DL, et al. Quantification of articular cartilage in the knee with pulsed saturation transfer subtraction and fat-suppressed MR imaging: optimization and validation. *Radiology* 1994;192 : 485-491
98. Kim DK, Ceckler TL, Hascall VC, Calabro A, Balaban RS. Analysis of water-macromolecule proton magnetization transfer in articular cartilage. *Magn Reson Med* 1993;29 : 211-215
99. Mlynarik V, Trattnig S, Huber M, Zembsch A, Imhof H. The role of relaxation times in monitoring proteoglycan depletion in articular cartilage. *J Magn Reson Imaging* 1999;10 : 497-502
100. Duvvuri U, Reddy R, Patel SD, Kaufman JH, Kneeland JB, Leigh JS. T1rho-relaxation in articular cartilage: effects of enzymatic degradation. *Magn Reson Med* 1997;38 : 863-867
101. Reddy R, Insko EK, Noyszewski EA, Dandora R, Kneeland JB, Leigh JS. Sodium MRI of human articular cartilage in vivo. *Magn Reson Med* 1998; 39:697 -701
102. Xia Y, Farquhar T, Burton-Wurster N, Ray E, Jelinski LW. Diffusion and relaxation mapping of cartilage-bone plugs and excised disks using microscopic magnetic resonance imaging. *Magn Reson Med* 1994; 31:273 -282
103. Mlynarik V, Sulzbacher I, Bittsanky M, Fuiko R, Trattnig S. Investigation of apparent diffusion constant as an indicator of early degenerative disease in articular cartilage. *J Magn Reson Imaging* 2003; 17:440 -444
104. Bashir A, Gray ML, Burstein D. Gd-DTPA2- as a measure of cartilage degradation. *Magn Reson Med* 1996;36 : 665-673
105. Bashir A, Gray ML, Boutin RD, Burstein D. Glycosaminoglycan in articular cartilage: in vivo assessment with delayed Gd(DTPA)(2-)-enhanced MR imaging. *Radiology* 1997;205 : 551-558
106. Burstein D, Velyvis J, Scott KT, et al. Protocol issues for delayed Gd(DTPA)(2-)-enhanced MRI (dGEMRIC) for clinical evaluation of articular cartilage. *Magn Reson Med* 2001;45 : 36-41
107. Gillis A, Bashir A, Mckeon B, Scheller A, Gray ML, Burstein D. Magnetic resonance imaging of relative glycosaminoglycan distribution in patients with autologous chondrocyte transplants. *Invest Radiol* 2001; 36:743 -748
108. Allen RG, Burstein D, Gray ML. Monitoring glycosaminoglycan replenishment in cartilage explants with gadolinium-enhanced magnetic resonance imaging. *J Orthop Res* 1999;17 : 430-436
109. Burstein D, Bashir A, Gray ML. MRI techniques in early stages of cartilage disease. *Invest Radiol* 2000;35 : 622-638
110. Bacic G, Liu KJ, Goda F, Hoopes PJ, Rosen GM, Swartz HM. MRI contrast enhanced study of cartilage proteoglycan degradation in the rabbit knee. *Magn Reson Med* 1997;37 : 764-768
111. Winalski CS, Shortkroff S, Mulkern RV, Schneider E, Rosen GM. Magnetic resonance relaxivity of dendrimer-linked nitroxides. *Magn Reson Med* 2002; 48:965 - 972
112. Grunder W, Biesold M, Wagner M, Werner A. Improved nuclear magnetic resonance microscopic visualization of joint cartilage using liposome entrapped contrast agents. *Invest Radiol* 1998; 33:193 -202
113. Wagner M, Werner A, Grunder W. Visualization of collagenase-induced cartilage degradation using NMR microscopy. *Invest Radiol* 1999; 34:607 -614

Reprint Address

M. P. Recht (rechtm@ccf.org)

Michael P. Recht,¹ Douglas W. Goodwin,² Carl S. Winalski,³ and Lawrence M. White⁴

¹Cleveland Clinic Foundation, 9500 Euclid Ave., A21, Cleveland, OH 44195

²Dartmouth-Hitchcock Medical Center, One Medical Center Dr., Lebanon, NH 03756

³Cartilage Repair Center and Department of Radiology, Brigham and Women's Hospital, 75 Francis St., Boston, MA 02115

⁴Mount Sinai Hospital, 600 University Ave., #563, Toronto, ON M5G 1X5, Canada

